CD38^{+} Endothelial Remodeling Defines Spatially Diverse Vasculopathy Programs in Rapidly Advancing Oral Inflammation

Quinn T. Easter[1], Khoa L. A. Huynh[2], Camila Schmidt Stolf[3], Jialiu Xie[4], Bruno F. Matuck[1], Akira Hasuike[5], Zabdiel Alvarado-Martinez[6], Zhaoxu Chen[7], Apoena Aguiar Ribeiro[8], Nivedita Pareek[9], Andrea M. Azcarate-Peril[9], Di Wu[4,10], Renato Casarin[3,11], Kang I. Ko[7], Jinze Liu[2,12], Kevin M. Byrd[1,12*]

[1] Department of Oral and Craniofacial Molecular Biology, Philips Institute for Oral Health Research, Virginia Commonwealth University, Richmond, VA, USA.

[2] Department of Biostatistics, Virginia Commonwealth University, Richmond, VA, USA.

[3] Department of Prosthodontics and Periodontics, Piracicaba Dental School, University of Campinas, São Paulo, BR.

[4] Department of Biostatistics, Gillings School of Global Public Health, University of North Carolina at Chapel Hill, Chapel Hill, NC, USA.

[5] Department of Periodontology, Nihon University School of Dentistry, Tokyo, JP.

[6] Independent Contractor, Bethesda, MD, USA.

[7] Department of Periodontics, School of Dental Medicine, University of Pennsylvania, Philadelphia, PA, USA.

[8] Division of Diagnostic Sciences, Adams School of Dentistry, University of North Carolina at Chapel Hill, Chapel Hill, NC, USA.

[9] Center for Gastrointestinal Biology and Disease, School of Medicine, University of North Carolina at Chapel Hill, Chapel Hill, NC, USA.

[10] Division of Oral and Craniofacial Health Sciences Adams School of Dentistry, University of North Carolina at Chapel Hill, Chapel Hill, NC, USA.

[11] Department of Periodontics and Endodontics, University at Buffalo, School of Dental Medicine. Buffalo, NY, USA.

[12] VCU Massey Comprehensive Cancer Center, Virginia Commonwealth University, Richmond, VA, USA.

* Correspondence to kevinmbyrd@gmail.com (KMB)

ONE-SENTENCE SUMMARY: Integrated single cell and spatial multiomic profiling of rapidly advancing oral inflammatory diseases reveals a shared vasculopathy signature marked by $CD38^{+}$ endothelial cell remodeling, nominating vascular niches as disease drivers and informing potential therapeutic targets.

Abstract (249)

Oral inflammatory diseases affect nearly half of the global population. Among them, newly defined peri-implantitis and high-grade periodontitis represent rapidly advancing inflammatory disease types, marked by relatively rapid tissue destruction. Despite their prevalence, the cell mechanisms and spatial architecture driving this severity remain poorly understood. Focusing first on peri-implantitis versus low- and moderate-grade periodontitis, we applied microbial profiling, single-cell RNA sequencing (scRNA-seq), and spatial proteomics (sp-proteomics) to uncover shared pathogenic programs linked to accelerated niche breakdown. Furthermore, to preserve spatial fidelity, each tissue was anatomically orientated along the tooth– or implant–epithelial interface, analogous sites of disease origination. Laser capture microdissection followed by microbiome analysis of unique tissue compartments revealed reduced bacterial load and diversity in peri-implantitis stroma. We then expanded our version-1 Human Periodontal Atlas by integrating newly generated peri-implantitis scRNAseq data (36-total samples; 121395-cells), revealing widespread transcriptional alterations, including oxidative stress, hypoxic, and NAD^+ metabolism-associated signatures, primarily in a subpopulation of *TNFRSF6B*$^+$/*ICAM1*$^+$ post-capillary venules. We then performed high-resolution sp-proteomics (15-total samples; 337260-cells) and analyzed VEC states and associated neighborhoods via *AstroSuite* using newly developed tri-wise spatial analysis. This revealed CD34$^+$-VEC loss and CD38$^+$-VEC expansion almost exclusively in peri-implantitis. We extended this analysis to high-grade periodontitis. Mucosal biopsies from four lesion-affected and four unaffected sites within the same individuals (1:1 matched; 8-samples; 225137-cells) again demonstrated spatially restricted CD38$^+$-VEC remodeling exclusively in affected tissues, with similar vasculopathy front patterning. The findings nominate spatially distinct vasculopathy patterning as a hallmark of rapidly advancing oral inflammation and a targetable therapeutic axis.

Introduction (833)

Mucosal inflammatory diseases of the oral cavity affect billions of individuals globally and remain a major obstacle to precision oral medicine[1,2]. Their clinical heterogeneity and limited molecular characterization have long hindered the development of targeted interventions[3-5]. While the roles of immune cells in chronic inflammation are well-established[6], the contributions of structural cell types to these inflammatory diseases i.e., epithelial and stromal cells, remain less clearly defined. These cells form the foundation of the tissue microenvironment by establishing physical barriers and regulating nutrient exchange; however, emerging spatial multiomic approaches have illuminated how structural cells also coordinate immune cell recruitment and local tissue regulation[7-9]. This growing body of work suggests that structural cell dysfunction may not simply result from inflammation but may actively initiate and sustain pathogenic immune programs, including structural cell inflammatory memory programs[10-13]. However, despite these insights, the spatial and transcriptional reprogramming of structural cells during chronic disease progression, particularly in rapidly advancing lesions, remains poorly understood.

Among mucosal inflammatory diseases, those that follow a rapidly destructive course offer key insights into the mechanisms that drive unchecked tissue breakdown. Rapidly advancing oral inflammatory diseases, such as recently-defined peri-implantitis[14] and high-grade periodontitis (Stage III/Grade C; aka “generalized rapidly advancing periodontitis”)[15,16], provide a valuable opportunity to investigate how structural and immune cell dysfunction contribute to this pathology. Despite sharing clinical hallmarks with more indolent forms of periodontitis, these two lesions exhibit accelerated destruction of both soft and hard tissues, often in shorter timeframes and with limited therapeutic responsiveness[17,18]. These conditions disproportionately compromise structural integrity and lead to significant clinical morbidity, yet the molecular distinctions that separate them from slower-advancing forms remain poorly resolved.

Importantly, they arise in anatomically adjacent but biologically distinct niches, implant versus tooth, offering a unique comparative framework for exploring how local microenvironments influence inflammatory programming and tissue breakdown. As such, these lesions serve as ideal models to study how spatially compartmentalized structural cells contribute to chronic inflammation and rapid mucosal degradation.

To interrogate the structural and spatial programs underlying rapid mucosal tissue destruction, we developed a multi-cohort, cross-disease framework integrating histopathology, laser capture microbiome profiling, single-cell RNA sequencing (scRNA-seq), and high-resolution spatial proteomics. All tissue samples were anatomically oriented along the tooth or implant interface to preserve spatial fidelity and enable direct comparisons of disease initiation sites. We first focused on peri-implantitis versus periodontitis, demonstrating that peri-implantitis lesions in this cohort are larger and display altered stromal matrix deposition. We then developed a novel laser capture microdissection followed by whole-genome microbial sequencing protocol, revealing that, despite exhibiting more severe clinical and histological destruction, peri-implantitis lesions paradoxically contained lower microbial quantity and diversity than either periodontitis or healthy tissues, especially in the stroma, highlighting the importance of host-driven mechanisms in lesion expansion.

To further uncover disease-specific cell states and transcriptional programs in a rapidly progressive inflammatory disase, we expanded our v1 Human Periodontal Atlas by integrating newly generated scRNA-seq data from peri-implantitis samples, totaling 121,395 cells[8,19]. This integrated analysis revealed widespread transcriptional reprogramming across nearly all major cell types, including epithelial cells, fibroblasts, and vascular endothelial cells (VECs). Notably, VECs were markedly increased in number within the disease-associated stroma, forming a distinct vascular compartment. This population exhibited upregulation of signaling pathways related to EGFR, insulin, leptin, IL-6, and B cell receptor activation. The most striking alterations

were found in a subpopulation of *TNFRSF6B*$^{+}$/*ICAM1*$^{+}$ post-capillary venules, which showed strong enrichment for oxidative stress, hypoxia, endothelial-to-mesenchymal transition (EndoMT), and NAD^{+}-related metabolic stress pathways, implicating this subset in the inflammatory vasculopathy unique to peri-implantitis.

To validate and spatially contextualize these findings, we applied high-resolution spatial proteomics (15-total samples; 337260-cells) and performed integrated analysis of VECs, immune cells, and their tissue cellular neighborhoods using *AstroSuite*, a containerized pipeline for multimodal spatial biology developed by our team[7,20]. For this multi-disease comparison, we developed a novel tri-wise spatial analysis framework capable of simultaneously comparing spatial distributions of cell types, cell states, and multicellular neighborhoods. Neighborhoods were computationally defined using *TACIT* and *Constellation*, two *AstroSuite* modules that infer cell types, states, and neighborhoods. This approach revealed disease-specific CD38^{+}-VEC expansion and CD34^{+}-VEC depletion almost exclusively in peri-implantitis. CD38^{+}-VECs formed immune-vascular interaction hubs characterized by close spatial proximity to cytotoxic T cells, helper T cells, and macrophages.

Given CD38's established role as an NAD^{+}-consuming ectoenzyme that regulates intracellular NAD^{+} levels and sirtuin signaling, its upregulation in VECs suggests a metabolic shift toward NAD^{+} depletion, oxidative stress and other vasculopathy phenotypes, congruent with transcriptomic enrichment for NAD^{+} metabolic dysregulation observed in peri-implant venules. To generalize these findings, we recruited a cohort of Stage III/Grade C periodontitis subjects, profiling 1:1 matched mucosal biopsies from lesion-affected and unaffected sites within the same individuals (8-total samples; 225137-cells). Again, CD38^{+} VEC remodeling was spatially restricted to affected tissues and displayed similar immune-vascular front patterning, suggesting convergent vasculopathy programs across both rapidly progressive diseases. Together, these findings identify spatially localized endothelial remodeling, marked by CD38-mediated NAD^{+}

metabolic stress, as a defining feature of rapidly advancing oral inflammation and nominate it as a potential targetable axis for intervention.

Results (3382)

A Multimodal Strategy to Understand Accelerated Oral Inflammatory Diseases.

Understanding why some oral inflammatory lesions progress rapidly while others remain indolent requires a deeper investigation into the molecular and spatial interplay between tissue-resident structural cells, immune infiltration, and microbial communities. While conventional diagnostics rely primarily on clinical and radiographic findings, these approaches fail to capture the complex biological heterogeneity underlying lesion behavior. To address this, we designed a multi-omics strategy to dissect the cellular and molecular architecture of these lesions across multiple layers of biological organization (Figure 1a). We employed histomorphometrics as well as laser capture microdissection (LCM) over epithelial and stromal compartments, followed by whole-genome microbial sequencing to assess microbial quantity and spatial distribution within healthy and inflamed tissues. We also used single-cell RNA sequencing (scRNA-seq) to define transcriptional programs of structural and immune cell types at high resolution by integrating into the human periodontal cell atlas. Finally, we leveraged high-dimensional spatial (sp)-proteomics to validate and contextualize these findings within intact tissue architecture. By integrating these orthogonal data types, we aimed to identify disease-specific cellular reprogramming, microbial-structural cell interactions, and proteomic remodeling events that together define the pathogenesis of rapidly destructive oral inflammation.

Histomorphometric Features Distinguish Peri-implantitis to Motivate Multiomics Profiling

To make head-to-head comparisons on rapidly advancing versus more slowly advancing, chronic lesions, we decided to first incorporate peri-implantitis into our growing oral and craniofacial atlasing efforts[7,21]. Peri-implantitis is a relatively recently defined inflammatory

disease that affects the soft and hard tissues surrounding dental implants[22]. While implant dentistry has seen remarkable success and long-term survival rates in most patients[23], a subset of implants develops peri-implantitis, which is characterized by mucosal inflammation, progressive bone loss, and eventual implant failure[14]. The disease presents a unique clinical challenge due to its frequently more rapid rate of progression, larger lesion size, and significantly higher densities of innate and adaptive immune cell types compared to periodontitis[24]. Despite its prevalence[25], the biological mechanisms that drive peri-implantitis remain incompletely understood[26].

To build on these findings and systematically interrogate the distinct tissue architectures of oral inflammatory disease, we curated a comparative cohort of human gingival biopsies from healthy individuals, patients with moderate (i.e., Stage II/III; Grade A/B) periodontitis, and patients with peri-implantitis, rigorously classified based on contemporary diagnostic criteria (Supplementary Table 1). This builds off our version 1.0 (v1) Human Periodontal Atlas, that includes health, gingivitis, and periodontitis samples, profiled using scRNAseq and/or spatial (sp)-transcriptomics, sp-proteomics, or sp-multiomic datasets[8,19]. We sought to confirm what has been known regarding peri-implantitis in our cohort to justify further investigation using an integrated multiomics approach.

We began by performing classical histological and histomorphometric analyses to assess lesion dimensions, epithelial organization, and immune-stromal interactions across conditions. Masson's trichrome staining revealed progressive tissue disorganization from health to disease (Figure 1b; Supplementary Figure 1a). Healthy gingiva exhibited an intact extracellular matrix (ECM) and epithelial barrier; periodontitis lesions showed ECM breakdown and immune infiltration at the tooth interface. Peri-implantitis lesions, however, demonstrated the most pronounced ECM degradation, with broad, deep immune infiltration and significant stromal remodeling. High-magnification images highlighted increased intermixing of immune (purple)

and stromal (blue) compartments in peri-implantitis, suggesting more extensive immune-stromal aggregation.

Hematoxylin and eosin (H&E) staining supported these observations (Supplementary Figure 1b), revealing limited immune infiltration in health (Figure 1c), largely confined to the deeper peri-crevicular and junctional zones. In contrast, both periodontitis and peri-implantitis samples exhibited substantial immune cell infiltration extending deep into the connective tissue, with lesions forming distinct localization patterns surrounding either the tooth (Figure 1d) or implant (three examples; Figure 1e). Quantitative morphometric analysis confirmed significant increases in lesion width and depth in peri-implantitis, exceeding those observed in periodontitis (Figure 1f, g). Although both disease states showed elevated lesion occupancy compared to health, only peri-implantitis demonstrated statistically significant increases across both horizontal and vertical dimensions, reinforcing its designation as a rapidly destructive lesion. Notably, even at this histological level, scattered vascular-like structures were more frequently observed throughout the peri-implantitis lesion, particularly within inflamed stromal regions (Figure 1b). These early histological cues confirmed known observations yet pointed toward increased vascular involvement, which justified deeper interrogation of the stromal compartment as a potentially overlooked contributor to lesion expansion and immune dysregulation.

Compartment-Resolved Microbiome Analysis Reveals Low Stromal Biomass in Peri-Implantitis

Peri-implantitis has long been recognized as having a distinct microbial profile compared to periodontitis[27]; however, it remains unknown whether its rapidly advancing phenotype is attributable to dysbiosis[28]. Additionally, we have recently observed tissue-level, cell type and spatial heterogeneity in microbial localization in periodontitis[8,19]. Since we observed increased vascular-like structures in peri-implantitis immune lesions (Figure 1, Supplementary Figure 1),

we hypothesized that peri-implantitis stroma might exhibit a higher bacterial burden than periodontitis, potentially driving exacerbated host responses related to local immune activation and tissue remodeling. To address this, we first used tissues sections for RNA fluorescence *in situ* hybridization (FISH), targeting bacterial *16S* rRNA to quantify microbial burden directly within FFPE tissue sections (Figure 2a). Unexpectedly, we observed that periodontitis samples consistently exhibited higher *16S* counts per cell across both epithelial and stromal compartments compared to peri-implantitis (Figure 2b,c).

To understand the diversity of the samples, we considered Shannon diversity to account for rare bacterial species, Simpson diversity to emphasize dominant species, richness to understand the number of distinct features, and evenness to determine how evenly individual counts were distributed among taxa (Figure 2d-h). We compared each of these four metrics across health, periodontitis, and peri-implantitis, considering combined compartments (epithelial- and stromal-specific compartments, Supplementary Figure 2). Across these indices, we found that in the combined data, there were comparatively few outliers, which resulted in no significant changes across any of the metrics. The widest variations occurred in healthy epithelia; this data is consistent with known microbiome composition differences in healthy individuals. We observed that while periodontitis and peri-implantitis epithelia had few differences, peri-implantitis stroma consistently had narrower indices than periodontitis stroma.

We then plotted the top enriched species, displaying compartments from least to most enriched (left to right; Figure 2i). No strong pattern emerged between diseases. We next extracted the top significant species across all 3 disease sets for comparison (Figure 2k). While we identified *Tannerella forsythia* as a top-represented species, we found few others that have been directly identified as contributing to pathogenesis. We reanalyzed the data for top contributing species using known periopathogens and asked whether any were enriched in periodontitis compared to peri-implantitis. While nearly all known periopathogens showed higher abundance in

periodontitis, only *Parvimonas sp. oral taxon 393* was statistically significant; the trend matched for epithelia. In stroma, a difference was noted for enriched *Filifactor alocis*, *Treponema medium*, and *Treponema vincentii*[29]. Thus, the accelerated tissue destruction seen in peri-implantitis likely did not stem from dysbiosis alone.

Vascular Endothelial Cell Dysfunction Emerges as a Core Pathogenic Feature in Peri-implantitis.

Peri-implantitis lesions have been reported to display prominent vascular density, often juxtaposed to immune cell infiltrates[24]; this is a pattern observable in our own histological datasets (Figure 1). This raised the possibility that vascular remodeling may be a core and underappreciated contributor to disease pathogenesis, distinct from classical immune-driven tissue destruction. To investigate this, we integrated scRNA-seq datasets from peri-implantitis patient biopsies with the v1 Human Periodontal Atlas (HPA), generating an updated composite reference that encompasses health, gingivitis, periodontitis, and peri-implantitis (Figure 3a; proportions, Supplementary Figure 3a). Integration using Harmony enabled improved alignment across datasets and was superior to Seurat-based methods for batch correction (Supplementary Figure 3b, c).

We then performed pseudobulk analysis of every major cell cluster after signature analysis (Supplementary Figure 3d), comprised of structural and immune cell types (Figure 3b; Supplementary Table 2). We performed differentially expressed gene (DEGs) analysis, and while there were many interesting trends upregulated in peri-implantits cell types compared to periodontitis, we focused on vascular endothelial cells (VECs) in peri-implantitis. Using this DEG list, pathway enrichment analysis revealed that peri-implantitis VECs exhibit a profound shift in both signaling and metabolic programs. We identified significant enrichment for growth factor

signaling (EGFR and KIT receptor pathways), hormonal regulation (insulin, leptin, and thyroid hormone signaling), and proinflammatory responses (IL-6, TROP2, TNF-α via NF-κB; Supplementary Data 2). Notably, NAD^+ metabolism and sirtuin signaling was selectively enriched in peri-implantitis VECs (Figure 3e, h).

The selective enrichment of NAD^+ metabolism and sirtuin signaling in peri-implantitis VECs suggests that they are not only activated but metabolically stressed, implicating energy depletion and impaired repair capacity as key contributors to the accelerated breakdown observed in peri-implantitis. This was confirmed by the significantly downregulated pathways in peri-implantitis VECs, including oxidative phosphorylation (OXPHOS), mitochondrial complex I and IV assembly, and electron transport chain activity (Supplementary Data 2). Suppression of these programs, alongside the upregulation of inflammation, hypoxia, and endothelial remodeling pathways, suggests a shift from quiescent vascular maintenance to a dysfunctional, inflamed, and energetically compromised state.

From this integrated dataset, we extracted the VEC compartment and performed high-resolution subclustering, resolving three canonical VEC subtypes: arteriolar (A-VECs), capillary (C-VECs), and post-capillary venular vascular endothelial cells (PCV-VECs) as we have previously done (Figure 3c)[30]. Marker gene analysis confirmed their identity: arterioles expressed *SAT1, CLDN5, SRGN*, and *CXCL12*; capillaries expressed *COL4A1 and PVLAP*; and PC-VECs expressed *SELP, SELE*, and *ACKR1* (Supplementary Figure 3e). DEG analysis comparing each subpopulation between peri-implantitis and periodontitis revealed that peri-implantitis-PCV-VECs were greatly affected, upregulating >1000 genes that were unique when compared to what was upregulated in A-VECs and C-VECs, which only displayed a small fraction of DEGs (Figure 3d). This pointed to PCV-VECs being a significant contributor to the endothelial cell dysfunction observed in peri-implantitis. When considering genes for hypoxia (*HIF1A*), NAD+

synthesis (*NAMPT*), and other genes related to NAD+ metabolism (*FOXO1, FOXO3, RIPK1, UBE4B*), we found that these were almost exclusively concentrated in a subregion of PCV-VECs.

To be better understand these cells, we performed a Tier 4 cell type analysis using clustered regions from Leiden clustering. We found two types of A-VECs (1: *CXCL12*$^{+}$*; IL32*$^{+}$ and 2: *IGF2*$^{+}$*, IGFBP3*$^{+}$), two types of C-VECs (1: *GSN*$^{+}$*, TIMP3*$^{+}$ and 2: *COL4A1*$^{+}$ *and RGCC*$^{+}$) and three types of PCV-VECs (1: *CCL14*$^{+}$*, CLU*$^{+}$*;* 2: *IER*$^{+}$*, NFKBIA*$^{+}$*;* and 3: *TNFSFR6*$^{+}$*, ICAM1*$^{+}$). It was these latter PCV-VECs that aligned with the NAD+ metabolism (Supplementary Table 2). We then repeated DEG analysis of these *TNFSFR6*$^{+}$/*ICAM1*$^{+}$ PCV-VECs, finding in inflammation compared to health many upregulated genes within this cluster (Figure 3g). Pathway enrichment analysis of *TNFRSF6B*$^{+}$/*ICAM1*$^{+}$ PCV-VECs revealed a variety of disease-relevant programs, including endothelial-to-mesenchymal transition, TNF-α/NF-κB signaling, TGF-β signaling, hypoxia, and IFN-related inflammatory responses (Figure 3h). These signatures implicate PCV-VECs not only as passive conduits but as active participants in immunovascular signaling, potentially sustaining chronic inflammation in peri-implant lesions. Unlike traditional models of periodontal disease centered on immune cells or microbial dysbiosis, these data suggest that vascular cells themselves may initiate or perpetuate tissue pathology.

Endothelial Remodeling and CD38^{+} *Vascular Expansion Define Peri-Implantitis Immune Niches.*

Having discovered VECs as important cell types for peri-implantitis pathogenesis, we decided to investigate the spatial immune and stromal architecture underlying peri-implantitis pathogenesis using sp-proteomics. Using healthy and periodontitis samples from our HPA v1.1[8], we performed the Phenocycler-Fusion assay (Akoya Biosciences) on peri-implantitis tissues (Figure

4a). Our 32-antibody CODEX panel targeted lineage, state, and activation markers for epithelial, stromal, and immune compartments, including VECs (Figure 4b). Following acquisition, we implemented a deep-learning segmentation model trained on multi-input features, including DAPI and membrane markers, enabling accurate single-cell segmentation across complex inflammatory niches (Figure 4c).

We then began generating cell recipes using the structural and immune markers in periodontitis and peri-implantitis (Figure 4d; health, Supplementary Figure 4). PanCK$^+$/KRT14$^+$ marked epithelial cells, whereas stromal cells were marked by vimentin (VIM$^+$); Ki67$^+$ identified cycling and non-cycling cells within each. We initially refined endothelial cells by classifying CD31$^+$ cells into VECs, VEC progenitor (CD34$^+$), and lymphatic endothelial cells (LECs; PDPN$^+$). Using CD45$^+$ as the overarching immune cell marker, in combination with antigen-presenting (HLA-A$^+$/HLA-DR$^+$), we classified adaptive CD3E$^+$ T cells and CD20$^+$ B cells and innate CD56$^+$ NK cells, CD11c$^+$/CD141$^+$ dendritic cells, myeloperoxidase (MPO$^+$) neutrophils, and CD68$^+$ macrophages. T cells were further refined into cytotoxic (CD8$^+$), helper (CD4$^+$), and regulatory (CD4+/FOXP3$^+$) T cell types.

Initial inspection of pan-CK$^+$ epithelium and surrounding VIM$^+$ stroma revealed significant expansion of disorganized, CD31$^+$ vasculature in peri-implantitis relative to periodontitis (Figure 4d-g). VECs exhibited partial loss of endothelial identity and increased expression of mesenchymal markers (e.g., VIM) without concomitant expression of other vasculature markers (e.g., PDPN, SMA), consistent with an EndoMT-like phenotype that may exacerbate tissue fibrosis and immune cell recruitment. This prompted focused evaluation of VECs and their phenotypic diversity. CD31$^+$ VECs in peri-implantitis lesions exhibited frequent co-expression of CD38, a marker associated with inflammation and NAD$^+$ metabolism in immune[31] and endothelial cells[32]. CD38$^+$ VECs were CD20-negative, and absent or rare in healthy or

periodontitis tissues (Figure 4d–g). Importantly, this expansion was not paralleled by a rise in $CD34^+$ VEC progenitors per area (Figure 4h,i), suggesting that $CD38^+$ endothelial remodeling reflects an inducible, disease-specific cell state rather than a developmental program.

To further characterize the immune-stromal niches enriched in peri-implantitis, we deployed the *AstroSuite* pipeline (*TACIT*, *Constellation*, and *Astrograph*)[7,20], which integrates spatial cell annotations, tissue compartment mapping, and spatial multiomics analyses (see Supplementary Information). Using Voronoi-based neighborhood reconstruction, we resolved spatial relationships among immune cells ($CD8^+$ T cells, macrophages, Tregs), structural elements (keratinocytes, LECs, fibroblasts), and VEC subsets. On a qualitative basis, as expected, the peri-implantitis immune lesion was dramatically larger than the periodontitis lesion (quantitative; Figure 1g); however, this also revealed an expansion of $CD38^+$ VECs in peri-implantitis, displaying multiple perivascular immune niches and vascular islands that were found to be distal to the originating lesion in peri-implantitis, (Figure 4j). These findings identify $CD38^+$ endothelial remodeling as a hallmark of peri-implantitis and highlight the utility of spatial proteomics and *AstroSuite* in resolving complex vascular-immune niches.

$CD38^+$ Endothelial Cell Niches Distinguish the Spatial Architecture of Peri-Implantitis

We next asked how $CD38^+$ vascular endothelial cells (VECs) were spatially organized in peri-implantitis and whether they co-occurred with specific immune or stromal populations (Figure 5a). To explore this, we included $CD31^+/CD38^+$ VECs as a distinct cell identity in our *TACIT*-based pipeline. Triwise enrichment analysis comparing *TACIT*-assigned cell types across health, periodontitis, and peri-implantitis revealed that $CD38^+$ VECs, $CD31^+/CD34^+$ VEC progenitors, and $CD31^+/CD38^-$ classical VECs were most enriched in peri-implantitis (Figure 5b). In contrast, immune cells, such as B cells, helper T cells, macrophages, and neutrophils,

were more concentrated in the lesions of both diseases. Periodontitis samples were more relatively enriched for NK cells, cytotoxic T cells, and dendritic cells. Both disease states also showed a relative depletion of epithelial and regulatory T cells compared to healthy tissue. These patterns were confirmed in lesion-wide bar plots, highlighting $CD38^+$ VECs as the most defining cell population in peri-implantitis (Figure 5c). Further, when we analyzed immune and vascular activation, $CD38^+$ VECs were frequently enriched for IFNγ (Supplementary Figure 5).

To analyze the spatial architecture of peri-implantitis, we used *AstroSuite*'s *Constellation* tool to assign cells to 11 tissue-connected neighborhoods (TCNs) based on co-occurrence and proximity (Figure 5d). Healthy samples were enriched for TCNs G and I; periodontitis for TCNs D and K; and peri-implantitis for TCNs A, F, and H (Figure 5e). $CD38^+$ VECs were prominently represented in TCNs A, F, and J: TCN A was an exclusion zone composed nearly entirely of $CD38^+$ VECs; TCN F showed $CD38^+$ VECs intercalating with classical VECs, VEC progenitors, and cytotoxic T cells; and TCN J consisted of $CD38^+$ VECs adjacent to fibroblasts. These findings revealed two distinct spatial modes for $CD38^+$ VECs in peri-implantitis: self-contained vascular niches and intercalated vascular-immune niches.

Next, we evaluated how these neighborhoods restructured tissue-wide architecture (Figure 5f). In health, a balanced network of six interconnected TCN hubs (A, C, D, G, J, K) with three or more connections to other TCNs supported tissue homeostasis. Analyzed periodontitis tissues apparently lost a “homeostatic” hub A and gained pathologic one, hub H, which we found is a new immune-rich stromal hub near the lesion front containing macrophages, T cells, and VECs. In peri-implantitis, TCNs A, D, G, and K were lost as hubs and replaced by TCNs H and F. TCN F formed a novel vascular-immune hub dominated by $CD38^+$ and classical VECs and cytotoxic T cells, indicating that vasculature was central to tissue remodeling in peri-implantitis.

To further characterize each TCN, we examined cell composition (Figure 5g). TCN A was dominated by CD38$^+$ VECs and VEC progenitors; TCN F contained classical and CD38$^+$ VECs, VEC progenitors, and cytotoxic T cells; and TCN J included fibroblasts, LECs, and NK cells alongside CD38$^+$ VECs. TCN B and E were enriched for neutrophils and B cells, respectively. TCN C contained a mix of stromal and immune cells, such as B cells, helper and regulatory T cells, and LECs, suggesting it represented an ectopic lymphoid structure. TCN H was enriched for macrophages and all T cell subtypes, whereas TCNs G and K marked transitional and structural stroma, respectively. These data reveal that CD38$^+$ VECs in peri-implantitis are embedded within structurally distinct spatial neighborhoods that alter hub connectivity and stromal-immune architecture. Rather than simply increasing in number, CD38$^+$ VECs reorganize the lesion's spatial framework, establishing exclusion and intercalation zones that shape the immune landscape of chronic disease. Furthermore, this recurring alignment between CD38$^+$ VECs and cytotoxic T cells within TCN F suggests a specialized vascular-immune niche that may coordinate immune effector positioning and tissue remodeling in peri-implantitis, highlighting a spatially orchestrated vascular expansion as well as vasculopathy.

Convergent CD38$^+$ Endothelial Pathology in Rapidly advancing Periodontitis and Peri-implantitis

To test whether the CD38$^+$ vasculopathy and stromal-immune remodeling observed in peri-implantitis are unique to the implant microenvironment or instead represent a broader pathological motif in destructive oral inflammatory diseases, we examined tissues from patients with Stage III, Grade C periodontitis. This rapidly advancing form of periodontitis is characterized by rapid tissue breakdown, even in systemically healthy individuals, offering an opportunity to assess whether similar spatial vascular-immune modules exist in natural-tooth disease. We collected matched gingival biopsies from unaffected and affected sites within the same individual (Figure 6a) and first evaluated tissue architecture using hematoxylin and eosin (H&E) staining. Compared to unaffected regions, affected sites exhibited clear histopathological

features of disease, including stromal expansion, dense leukocyte infiltration, and epithelial rete ridge broadening (Figure 6b). These histological signatures resembled those observed in peri-implantitis and prompted spatial proteomic profiling using the sp-proteomics (Akoya PhenoCycler Fusion) panel.

High-plex imaging revealed consistent expansion of $CD31^+/CD38^+$ VECs in affected Grade C tissues, localized prominently in connective tissue regions beneath the sulcus and junctional epithelium (Figure 6c). These $CD38^+$ VECs frequently appeared as organized vascular clusters co-localizing with $CD45^+$ leukocytes and basal epithelial zones (Figure 6d), forming similar patterns of vascular remodeling observed in peri-implantitis yet not in matched healthy sites (Figure 6e,f). To probe for features of endothelial plasticity similar to peri-implantitis, we assessed co-expression of CD38 with stromal markers. We observed upregulation of vimentin (VIM) in $CD38^+$ VECs in affected—but not unaffected—tissue regions, without upregulation of PDPN or SMA and lack of expansion of CD34, consistent with endothelial-to-mesenchymal transition (EndoMT) (Figure 6g–j). Additionally, we observed similar counts of CD38 per lesion measurement area when compared to peri-implantitis (Figure 6k), suggesting that $CD38^+$ vasculature in Grade C lesions may also participate in immune guidance and undergo structural remodeling.

To understand the cell distribution within tissues, we applied our *AstroSuite* pipeline to both the healthy and affected sites (Figure 6l). In affected tissues, we observed an expanding $CD38^+$ VEC front similar to peri-implantitis. To uncover any shared features, we employed our triwise enrichment analysis of *TACIT*-assigned cell types to compare low-grade (B) periodontitis, peri-implantitis, and high-grade (C) periodontitis (Figure 6m). We found that across all three disease states, only $CD38^+$ VECs were shared between peri-implantitis and Grade C periodontitis. Further, spatial mapping revealed frequent co-localization of $CD38^+$ VECs and $CD8^+$ cytotoxic T cells within the same tissue niches (Figure 6n). These immune-vascular neighborhoods were

repeatedly observed in affected sites and were notably absent in unaffected tissues. This mirrors the peri-implantitis phenotype, where $CD38^+$ vasculature interfaces directly with immune effectors, specifically CD8+ cytotoxic T cells. The recurrence of these patterns across disease types suggests a conserved stromal-immune architecture underpinning destructive inflammation in the oral cavity. Overall, these data extend our findings beyond peri-implantitis and support a model in which $CD38^+$ VEC expansion, EndoMT, and selective immune cell coupling form a shared spatial program in rapidly progressive inflammatory lesions.

Discussion (934)

The oral cavity presents a powerful yet underutilized model for investigating tissue remodeling in human disease. Here, mechanical stress, polymicrobial exposure, and continuous immune surveillance converge within an anatomically confined, readily accessible tissue. Unlike many mucosal surfaces, the oral mucosa exhibits both rapid and spatially restricted inflammatory dynamics, offering a rare opportunity to observe lesion development in real time—from acute shifts over days to long-term remodeling over months or years. Leveraging these advantages, we conducted what we believe to be the first spatial omics study of both peri-implantitis and Stage III/Grade C periodontitis. This integrated multi-disease spatial analysis, which we believe is among the first of its kind in the spatial biology era, uncovered a shared immunovascular pathology defined by the expansion of $CD38^+$ vascular endothelial cells. These cells do not merely reflect downstream inflammation but actively reshape the tissue landscape by forming discrete, lesion-specific spatial modules that couple with cytotoxic T cells and disrupt classical fibrovascular architecture.

A review of the literature underscores that endothelial cell biology remains understudied in oral inflammatory diseases. Most of the limited spatial or single-cell omics studies in the field have focused on immune, fibroblast, and/or epithelial dynamics, while vasculature is often treated as a static scaffold. Yet endothelial dysfunction plays a critical role in many chronic pathologies, where aberrant endothelial states reshape immune infiltration and tissue-specific immunity[33,34]. By anchoring our analysis around endothelial subtypes, we reveal that $CD38^+$ VECs emerge consistently in rapidly advancing oral lesions, co-occur with both innate and adaptive immune cells, and show signatures of IFNγ exposure and endothelial-to-mesenchymal transition (Supplementary Figure 5). These cells are not only expanded but spatially reorganized, forming distinct exclusion or intercalation zones across tissue compartments.

Between the two rapidly advancing diseases studied here, peri-implantitis is rising in prevalence alongside increased dental implant use, affecting roughly one-quarter of patients[25]; for a variety of factors, the prevalence of peri-implantitis is expected to increase[35]. Peri-implantitis is often characterized as a biofilm-driven inflammatory lesion, yet our findings revise this bacteria-centric view by revealing a consistent expansion of $CD38^+$ VECs and immune-coupled vascular hubs, despite relatively lower bacterial abundance in some high-grade cases. Importantly, the current therapeutic paradigms for peri-implantitis center on plaque control and debridement but have yielded limited success in halting disease progression[36]. We hypothesize that part of that limited success is because the host-response is uniquely shaping niche-specific tissue breakdown, which may be exacerbated but not driven by dysbiosis. Similarly, in Stage III/Grade C periodontitis, we observe parallel expansion of $CD38^+$ VECs and their association with cytotoxic T cells in the connective tissues. This form of periodontitis is also difficult to treat[16], a general feature of oral inflammation based on our current studies outside this niche.

This vascular-centric spatial phenotype introduces a new conceptual framework for understanding chronic oral disease and suggests novel therapeutic avenues. CD38 is an NAD^+-hydrolyzing ectoenzyme that also serves as an immune modulator. Its expression on endothelial cells has been implicated in inflammatory vasculopathies of the heart, brain, and kidneys[37-39]. Monoclonal antibodies against CD38 (e.g., daratumumab, isatuximab) are already FDA-approved for hematologic malignancies and could be repurposed, using local delivery strategies, to target pathogenic endothelial states in mucosal inflammation as they have been recently explored for autoimmunity[40-42]. Moreover, interventions aimed at restoring NAD^+ levels, activating SIRT1, or blocking IFNγ signaling, pathways observed in the $CD38^+$ VECs in our data, may blunt maladaptive vascular remodeling and its downstream immune effects. These

targets provide a translational bridge between spatial pathology and molecular precision therapeutics in oral medicine.

The diagnostic implications of our findings are equally significant. Traditional metrics for lesion severity focus on immune composition, microbial load, or tissue damage[43]. Yet our analysis shows that endothelial subtypes and their spatial arrangements better predict tissue organization and immune residency than immune proportions and stromal density alone. For instance, $CD8^+$ T cells co-occur with $CD38^+$ VECs in peri-implantitis and Grade C periodontitis but not in classical periodontitis, despite $CD8^+$ T cells and $CD38^+$ VECs being present in all three diseases. This indicates that spatial context, not just cell identity, determines immunopathology. Future diagnostic frameworks may incorporate vascular profiling to stratify disease subtypes and predict treatment response, a strategy applicable not only in the oral cavity but across mucosal diseases and disorders.

Despite its strengths, our study has limitations. The spatial omics analyses were performed on a carefully curated yet limited set of human tissue samples, reflecting the difficulty in acquiring high-quality peri-implant and Stage III/Grade C periodontitis lesions. While the consistency of $CD38^+$ VEC emergence across samples is striking, larger cohorts are needed to enable subtyping and longitudinal tracking. Additionally, the lack of healthy peri-implant mucosa or peri-implant mucositis samples constrains our ability to resolve early transitions in vascular remodeling. Finally, current animal models lack fidelity for replicating human-specific endothelial–immune interactions and NAD^+ metabolism from our experience, complicating preclinical translation.

Nonetheless, this study reframes vascular architecture as a central player in oral tissue inflammation and destruction. The emergence of $CD38^+$ VECs within two distinct diseases points to a shared vascular module that disrupts immune equilibrium and structural integrity.

These lesions are not merely consequences of immune overactivation or bacterial invasion, but spatially organized outcomes of endothelial rewiring. As spatial biology becomes increasingly integrated into translational science, we propose that vascular-centric frameworks may yield new insights across organ systems. The oral cavity, with its accessibility and spatiotemporal resolution, provides a powerful setting to pioneer these approaches. In our view, this spatial omics study lays the foundation for incorporating vascular profiling into the next generation of oral disease classification and treatment strategies, and potentially into broader models of mucosal pathobiology[44].

Materials and Methods (301)

Study design. This study aimed to characterize vascular contributions to human gingival inflammatory diseases peri-implantitis and Grade C periodontitis using an integrated approach of spatial transcriptomics, laser capture microdissection, and single-cell multiomic profiling. The objectives were to a) identify transcriptional signatures in vascular endothelial cells within diseased gingiva and b) to define cell neighborhoods that correlated with tissue inflammation and immune dysregulation.

Sample information. In total, we used 24 samples (4 health, 5 periodontitis, 7 peri-implantitis, 4 Grade C periodontitis and 4 matched health) acquired from adult humans around teeth or dental implants for these analyses. All samples were obtained under informed consent in accordance with the Declaration of Helsinki. We did not perform power analysis or establish rules for stopping data collection. Outliers were identified as samples with less than 500 unique genes/cell for single-cell RNA sequencing and less than 90% cell identification (TACIT) and were excluded from downstream analyses. Primary endpoints were spatial and transcriptional signatures of vascular endothelial cells in health and diseased tissues. Secondary endpoints included cell-cell interaction modeling from multiomic data. Biological replicates were gingival tissue from a minimum of 3 patients per group. Experimental replicates were a minimum of 3 per sample type. Histomorphometric and spatial proteomic analyses were performed on sequential sections.

Experimental design. This was a controlled observational study of clinical samples. Gingival tissues were collected during routine surgical procedures, fixed, embedded, sectioned, and subjected to histomorphometry, spatial proteomics, laser capture microdissection, and single-cell RNA sequencing protocols (see Supplementary Information for more detail).

Randomization and Blinding. Patients were stratified by disease classification. There was no randomization applied because this was an observational study. Tissue sections were randomly assigned for modality to minimize positional bias. Investigators were blinded to disease groups during data analysis, though each group contained specific features that indicated disease status.

References

1 Schifter, M., Yeoh, S. C., Coleman, H. & Georgiou, A. Oral mucosal diseases: the inflammatory dermatoses. *Australian dental journal* **55**, 23-38 (2010).

2 Armitage, G. C. Periodontal diagnoses and classification of periodontal diseases. *Periodontology 2000* **34**, 9-21 (2004).

3 Pinna, R. *et al.* Genetic and developmental disorders of the oral mucosa: Epidemiology; molecular mechanisms; diagnostic criteria; management. *Periodontology 2000* **80**, 12-27 (2019).

4 Hong, C. H. *et al.* World Workshop on Oral Medicine VII: Relative frequency of oral mucosal lesions in children, a scoping review. *Oral Diseases* **25**, 193-203 (2019).

5 Healy, C. M. & Galvin, S. Biological therapies and management of oral mucosal disease. *Br Dent J* **236**, 317-321 (2024). https://doi.org/10.1038/s41415-024-7065-9

6 Moutsopoulos, N. M. & Konkel, J. E. Tissue-Specific Immunity at the Oral Mucosal Barrier. *Trends Immunol* **39**, 276-287 (2018). https://doi.org/10.1016/j.it.2017.08.005

7 Matuck, B. F. *et al.* The Immunoregulatory Architecture of the Adult Oral Cavity. *bioRxiv*, 2024.2012.2001.626279 (2024). https://doi.org/10.1101/2024.12.01.626279

8 Easter, Q. T. *et al.* Single-cell and spatially resolved interactomics of tooth-associated keratinocytes in periodontitis. *Nature Communications* **15**, 5016 (2024).

9 Krausgruber, T. *et al.* Structural cells are key regulators of organ-specific immune responses. *Nature* **583**, 296-302 (2020). https://doi.org/10.1038/s41586-020-2424-4

10 Cheng, D. *et al.* New insights into inflammatory memory of epidermal stem cells. *Front Immunol* **14**, 1188559 (2023). https://doi.org/10.3389/fimmu.2023.1188559

11 Cadinu, P. *et al.* Charting the cellular biogeography in colitis reveals fibroblast trajectories and coordinated spatial remodeling. *Cell* **187**, 2010-2028.e2030 (2024). https://doi.org/10.1016/j.cell.2024.03.013

12 Gonsales Spindola, D. *et al.* Endothelial Cells retain inflammatory memory through chromatin remodeling. *bioRxiv*, 2025.2006. 2012.659136 (2025).

13 Hartlehnert, M. *et al.* Schwann cells promote post-traumatic nerve inflammation and neuropathic pain through MHC class II. *Sci Rep* **7**, 12518 (2017). https://doi.org/10.1038/s41598-017-12744-2

14 Berglundh, T. *et al.* Peri-implant diseases and conditions: Consensus report of workgroup 4 of the 2017 World Workshop on the Classification of Periodontal and Peri-Implant Diseases and Conditions. *J Clin Periodontol* **45 Suppl 20**, S286-s291 (2018). https://doi.org/10.1111/jcpe.12957

15 Tonetti, M. S., Greenwell, H. & Kornman, K. S. Staging and grading of periodontitis: Framework and proposal of a new classification and case definition. *J Periodontol* **89 Suppl 1**, S159-s172 (2018). https://doi.org/10.1002/jper.18-0006

16 Roshna, T. & Nandakumar, K. Generalized rapidly advancing periodontitis and its treatment options: case reports and review of the literature. *Case Rep Med* **2012**, 535321 (2012). https://doi.org/10.1155/2012/535321

17 Kwon, T., Lamster, I. B. & Levin, L. Current concepts in the management of periodontitis. *International dental journal* **71**, 462-476 (2021).

18 Roccuzzo, M., Layton, D. M., Roccuzzo, A. & Heitz-Mayfield, L. J. Clinical outcomes of peri-implantitis treatment and supportive care: A systematic review. *Clinical oral implants research* **29**, 331-350 (2018).

19 Easter, Q. T. *et al.* Polybacterial intracellular macromolecules shape single-cell inflammatory profiles in upper airway epithelia. *NPJ Biofilms Microbiomes* **11**, 100 (2025). https://doi.org/10.1038/s41522-025-00735-5

20 Huynh, K. L. A. *et al.* Deconvolution of cell types and states in spatial multiomics utilizing TACIT. *Nat Commun* **16**, 3747 (2025). https://doi.org/10.1038/s41467-025-58874-4
21 Caetano, A., Oral, H. C. A., Bionetwork, C., Sequeira, I. & Byrd, K. A roadmap for the human oral and craniofacial cell atlas. *Journal of Dental Research* **101**, 1274-1288 (2022).
22 Rokaya, D., Srimaneepong, V., Wisitrasameewon, W., Humagain, M. & Thunyakitpisal, P. Peri-implantitis Update: Risk Indicators, Diagnosis, and Treatment. *Eur J Dent* **14**, 672-682 (2020). https://doi.org/10.1055/s-0040-1715779
23 Moraschini, V., Poubel, L. A., Ferreira, V. F. & Barboza Edos, S. Evaluation of survival and success rates of dental implants reported in longitudinal studies with a follow-up period of at least 10 years: a systematic review. *Int J Oral Maxillofac Surg* **44**, 377-388 (2015). https://doi.org/10.1016/j.ijom.2014.10.023
24 Carcuac, O. & Berglundh, T. Composition of human peri-implantitis and periodontitis lesions. *J Dent Res* **93**, 1083-1088 (2014). https://doi.org/10.1177/0022034514551754
25 Diaz, P., Gonzalo, E., Villagra, L. J. G., Miegimolle, B. & Suarez, M. J. What is the prevalence of peri-implantitis? A systematic review and meta-analysis. *BMC Oral Health* **22**, 449 (2022). https://doi.org/10.1186/s12903-022-02493-8
26 Fragkioudakis, I., Tseleki, G., Doufexi, A. E. & Sakellari, D. Current Concepts on the Pathogenesis of Peri-implantitis: A Narrative Review. *Eur J Dent* **15**, 379-387 (2021). https://doi.org/10.1055/s-0040-1721903
27 Dabdoub, S. M., Tsigarida, A. A. & Kumar, P. S. Patient-specific analysis of periodontal and peri-implant microbiomes. *J Dent Res* **92**, 168s-175s (2013). https://doi.org/10.1177/0022034513504950
28 Kotsakis, G. A. & Ganesan, S. M. Microbial Dysbiosis, Titanium Release, and Peri-implantitis. *J Dent Res* **104**, 473-480 (2025). https://doi.org/10.1177/00220345241307939
29 Carvalho É, B. S., Romandini, M., Sadilina, S., Sant'Ana, A. C. P. & Sanz, M. Microbiota associated with peri-implantitis-A systematic review with meta-analyses. *Clin Oral Implants Res* **34**, 1176-1187 (2023). https://doi.org/10.1111/clr.14153
30 Huang, N. *et al.* SARS-CoV-2 infection of the oral cavity and saliva. *Nature medicine* **27**, 892-903 (2021).
31 Chini, C. C. S. *et al.* CD38 ecto-enzyme in immune cells is induced during aging and regulates NAD(+) and NMN levels. *Nat Metab* **2**, 1284-1304 (2020). https://doi.org/10.1038/s42255-020-00298-z
32 Qiu, Y. *et al.* NAD(+) exhaustion by CD38 upregulation contributes to blood pressure elevation and vascular damage in hypertension. *Signal Transduct Target Ther* **8**, 353 (2023). https://doi.org/10.1038/s41392-023-01577-3
33 Castellon, X. & Bogdanova, V. Chronic Inflammatory Diseases and Endothelial Dysfunction. *Aging Dis* **7**, 81-89 (2016). https://doi.org/10.14336/ad.2015.0803
34 Steyers, C. M., 3rd & Miller, F. J., Jr. Endothelial dysfunction in chronic inflammatory diseases. *Int J Mol Sci* **15**, 11324-11349 (2014). https://doi.org/10.3390/ijms150711324
35 Dreyer, H. *et al.* Epidemiology and risk factors of peri-implantitis: A systematic review. *J Periodontal Res* **53**, 657-681 (2018). https://doi.org/10.1111/jre.12562
36 Herrera, D. *et al.* Prevention and treatment of peri-implant diseases-The EFP S3 level clinical practice guideline. *J Clin Periodontol* **50 Suppl 26**, 4-76 (2023). https://doi.org/10.1111/jcpe.13823
37 Boslett, J., Hemann, C., Christofi, F. L. & Zweier, J. L. Characterization of CD38 in the major cell types of the heart: endothelial cells highly express CD38 with activation by hypoxia-reoxygenation triggering NAD(P)H depletion. *Am J Physiol Cell Physiol* **314**, C297-c309 (2018). https://doi.org/10.1152/ajpcell.00139.2017

38 Tao, Y. *et al.* Comprehensive Proteomics Analysis Identifies CD38-Mediated NAD(+) Decline Orchestrating Renal Fibrosis in Pediatric Patients With Obstructive Nephropathy. *Mol Cell Proteomics* **22**, 100510 (2023). https://doi.org/10.1016/j.mcpro.2023.100510

39 Yu, M. *et al.* Targeting CD38 to alleviate brain endothelial cell dysfunction and cognitive impairment in vascular dementia. *J Pharmacol Sci* **158**, 310-321 (2025). https://doi.org/10.1016/j.jphs.2025.05.013

40 Ye, X. *et al.* The potential of CD38 protein as a target for autoimmune diseases. *Autoimmun Rev* **22**, 103289 (2023). https://doi.org/10.1016/j.autrev.2023.103289

41 Benfaremo, D. & Gabrielli, A. Is There a Future for Anti-CD38 Antibody Therapy in Systemic Autoimmune Diseases? *Cells* **9** (2019). https://doi.org/10.3390/cells9010077

42 van de Donk, N. W. *et al.* Monoclonal antibodies targeting CD38 in hematological malignancies and beyond. *Immunol Rev* **270**, 95-112 (2016). https://doi.org/10.1111/imr.12389

43 Kinane, D. F., Stathopoulou, P. G. & Papapanou, P. N. Periodontal diseases. *Nat Rev Dis Primers* **3**, 17038 (2017). https://doi.org/10.1038/nrdp.2017.38

44 Revach, O. Y. *et al.* Overcoming resistance to immunotherapy by targeting CD38 in human tumor explants. *Cell Rep Med* **6**, 102210 (2025). https://doi.org/10.1016/j.xcrm.2025.102210

Figure 1. Histomorphometric analysis reveals characteristic features of periodontitis and peri-implantitis immune lesions. a) Overview of multiomic dissection of accelerated oral mucosal inflammation in this study. b) Masson's trichrome staining of biopsies enables identification of structural-immune features, including ECM loss in peri-implantitis. H&E images of c) health, d) periodontitis, and e) peri-implantitis biopsies indicated larger immune lesions in peri-implantitis. f) Schematic of parameters used to quantify immune lesion analysis. g) Statistical analysis of length and area scales of width, horizontal and vertical length, depth, and ROI showed peri-implantitis differed from periodontitis across all metrics; lesion occupancy showed no difference. Scale bars: a), b), c), f) 300 µm; f) (inset) 20 µm; g) 50 µm. Statistical analysis: g) $*p < 0.05$. N = 4 (health), 5 (periodontitis), 7 (peri-implantitis). Images in a) were generated using BioRender.

Figure 2. Dybiosis is not a major contributor to peri-implantitis pathogenesis. a) Using a probe for *16S* rRNA, we observed lower enrichment of bacterial signal in peri-implantitis epithelia and stroma. b) H&E images showing areas from which laser capture microdissection (LCM) samples were acquired. c)-g) represent first-in-class whole-genome sequencing-derived data of FFPE-derived LCM sections. c) We found few unique represented species comparing periodontitis and peri-implantitis. d) Alpha-beta diversity of represented species across health and diseases showed no significant species. e) Shannon and Simpson diversity indices, including richness and evenness across health and diseases, showed that while health differed from both periodontitis and peri-implantitis, in general, peri-implantitis had less diversity. f) Top represented species across health, periodontitis, and peri-implantitis samples. g) Directly comparing periodontitis and peri-implantitis for top-represented pathogens, only one species (*Parvimonas spp.*) was enriched in periodontitis; no other species statistically differed between the diseases. Scale bar: b) 20 µm For g) $p < 0.0005$. Images in a) were generated using BioRender.

Figure 3. Integration of single-cell RNA sequencing (scRNAseq) data reveals shared vascular populations across health and disease. a) Our Human Periodontal Atlas (HPA) v1. b) Integration of peri-implantitis scRNAseq data resulted in our HPA v1.1. c) Focusing on the vasculature, we identified arterioles (A-VECs), capillaries (C-VECs), and post-capillary venules (PC-VECs). d) PC-VECs expressed more unique genes in peri-implantitis. e) differentially expressed gene analysis of arterioles, capillaries, and post-capillary venules revealed NAD^+-associated metabolism in PCVs. f) Reannotation of VECs revealed among 8 subpopulations, a subpopulation of *TNFRSF6*$^+$/*ICAM1*$^+$ PC-VECs expressed the NAD^+-associated metabolism genes in e). g) Differentially expressed genes (DEGs) of *TNFRSF6*$^+$/*ICAM1*$^+$ PC-VECs. h) Classifying the DEGs using MSigDB revealed inflammatory response, hypoxia, and TNF-alpha signaling as top represented pathways.

Figure 4. Highly multiplexed immunofluorescence unveils the immune heterogeneity in periodontitis and peri-implantitis. a) Schematic of immunophenotyping of health, periodontitis, and peri-implantitis. b) Conjugated antibody library used in this study to distinguish cell identity and state. c) We trained CellPose for cell segmentation based on DAPI to enable precise fluorescence calls. d)-g) Regional immunophenotypes of the junction and sulcus in d) periodontitis were defined by e) immune expansion, yet in f) peri-implantitis, g) $CD31^+/VIM^+$ vascular cells expanded without additional identifying markers. h)-i) $CD31^+/CD34^+$ progenitor cells were present in both tissue types, yet we observed expansion of $CD31^+/CD38^+$ VECs in peri-implantitis lesions. j) Using our AstroSuite pipeline, we used the segmented data to generate Voronoi masks of supervised, defined cell types. Scale bars: d)-g): 50 µm; h): 20 µm. Statistical analysis: i) $^{**}p < 0.005$. Images in a and j were generated using BioRender.

Figure 5. Peri-implantitis tissue-connected neighborhood proportions and spatial localizations define a unique pathology dominated by CD38 VECs. a) Schematic of different cell environments surrounding $CD38^+$ VECs in periodontitis and peri-implantitis. b)

Triwise enrichment comparison of health, periodontitis and peri-implantitis revealed the periodontitis/peri-implantitis group was enriched for most immune cell types, yet peri-implantitis was strongly enriched for $CD38^+$ VECs. c) Proportions of cells across health and disease states. d) Proportions of TCNs within health and disease states. e) Voronoi representations of healthy, periodontitis, and peri-implantitis tissue connected neighborhoods (TCNs). Peri-implantitis shows expansion of $CD38^+$ VECs through TCNs A, F, and H. f) TCN interaction hubs are dominated by $CD38^+$ VEC neighborhoods in peri-implantitis. g) Analysis of Cell x TCN information revealed five hubs enriched for $CD38^+$ VECs; TCNs A, F, and H all expand in peri-implantitis. Images in a) were generated using BioRender.

Figure 6. $CD38^+$ vasculopathy is a feature of Stage III/Grade C periodontitis. a) Schematic showing same-person collection of unaffected and affected tissues. Triwise plot showing enriched cell types shared between different tissue states. b) H&E analysis shows affected sites display significantly higher cellular density. c)-f) Regional immunophenotypes of affected and unaffected sites show that c) Grade C periodontitis lesions display immune infiltrant and d) $CD31^+$ expansion, while e),f) unaffected sites appear comparatively healthy. g) Inspection of the expanding $CD31^+$ lesions revealed $CD38^+$, not $CD34^+$ VEC enrichment. h),i) We further observed these cells were h) $CD31^+/VIM^+$ in affected sites and i) were not enriched for other vascular identifying markers. j) Grade C periodontitis sites were enriched for $CD31^+/CD38^+$ VECs. k) We observed no differences in lesion density of $CD31^+/CD38^+$ VECs in peri-implantitis and Grade C periodontitis. l) We applied our AstroSuite toolkit to unaffected and unaffected sites and observed tissue-wide expansion of $CD38^+$ VECs. m) Triwise analysis of three disease types revealed peri-implantitis and Grade C periodontitis were enriched for $CD38^+$ VECs. n) Both diseases shared the predicted $CD38^+$ VEC/CD8 T cell neighborhood predicted by Constellation. Scale bars: c)-f): 50 µm; g)-i), n): 20 µm. Statistical analysis: j) $*p < 0.05$. Images in a and l were generated using BioRender.

List of Supplementary Materials

Supplementary Information. Additional information for materials and methods.

Figure 1S. Masson's and H&E images of health, periodontitis, and peri-implantitis biopsies.

Figure 2S. Epithelial- and stromal-specific alpha- and beta-diversity analyses.

Figure 3S. Proportions of cell types per condition, additional clustering types, and differentially expressed gene plots for all and vascular endothelial cell subpopulations.

Figure 4S. Healthy mIF data acquired from PhenoCycler Fusion.

Figure 5S.

Supplementary Table 1. Metadata for health, periodontitis, peri-implantitis, Grade C periodontitis, and matched healthy samples.

Supplementary Table 2. Differentially expressed gene lists for Tier 1 cell sets and Tier 2 vascular endothelial cell subpopulations.

Acknowledgements, Funding, Author Contributions, and Competing Interests. We would like to acknowledge the NIH/NIDCR Dental Clinic, specifically Rachel Adam, Danielle Elangue, and Janice Lee, for their continued support to provide human tissues. Services in support of this work were provided by the VCU Massey Comprehensive Cancer Center Bioinformatics Shared Resource, supported in part with funding from the NIH-NCI Cancer Center Support Grant (#P30CA016059). The UNC Microbiome Core is funded in part by the Center for Gastrointestinal Biology and Disease (CGIBD P30 DK034987) and the UNC Nutrition Obesity Research Center (NORC P30 DK056350). Peri-implant tissue acquisition was partly funded by the Schoenleber Grant from the UPenn Oral Maxillofacial Surgery Department to KIK. This work was supported by the Fundação de Amparo à Pesquisa do Estado de São Paulo (FAPESP; #2021/11082-4) to CSS, Nihon University (2022 Overseas Researcher Grant) to AH, the National Institute of Dental and Craniofacial Research (#1R03DE034507-01) to DW, and generous start-up funds from the ADA Science & Research Institute (Volpe Research Scholar Award) and the Philips Institute for Oral Health Research, as well as the American Academy of Implant Dentistry Foundation (Large Research Grant) to KMB. For this study, KMB and QTE conceptualized the project. QTE, KLAH, JX and AH developed methods for project analysis. Janice Lee (National Institute of Dental, Oral & Craniofacial Research), KIK, and RC supported the recruitment of patients and collected data. QTE, CSS, ZC, KIK, RC & KMB collected samples for analysis. QTE, KLAH, JX, BFM, AH, ZAM, AAR, NP, AMA-P & KMB performed experimental and/or bioinformatic analysis. QTE and KMB wrote the original draft; all authors critically reviewed and edited the final manuscript. The authors had access to the study data and reviewed and approved the final manuscript. Although the authors view each of these as noncompeting financial interests, KMB, QTE, BFM, and AH are all active members of the Human Cell Atlas; furthermore, KMB is a scientific advisor at Arcato Laboratories, and JL and KMB are co-founders and KMB is CEO of Stratica Biosciences. All other authors declare no competing interests.

Figure 1

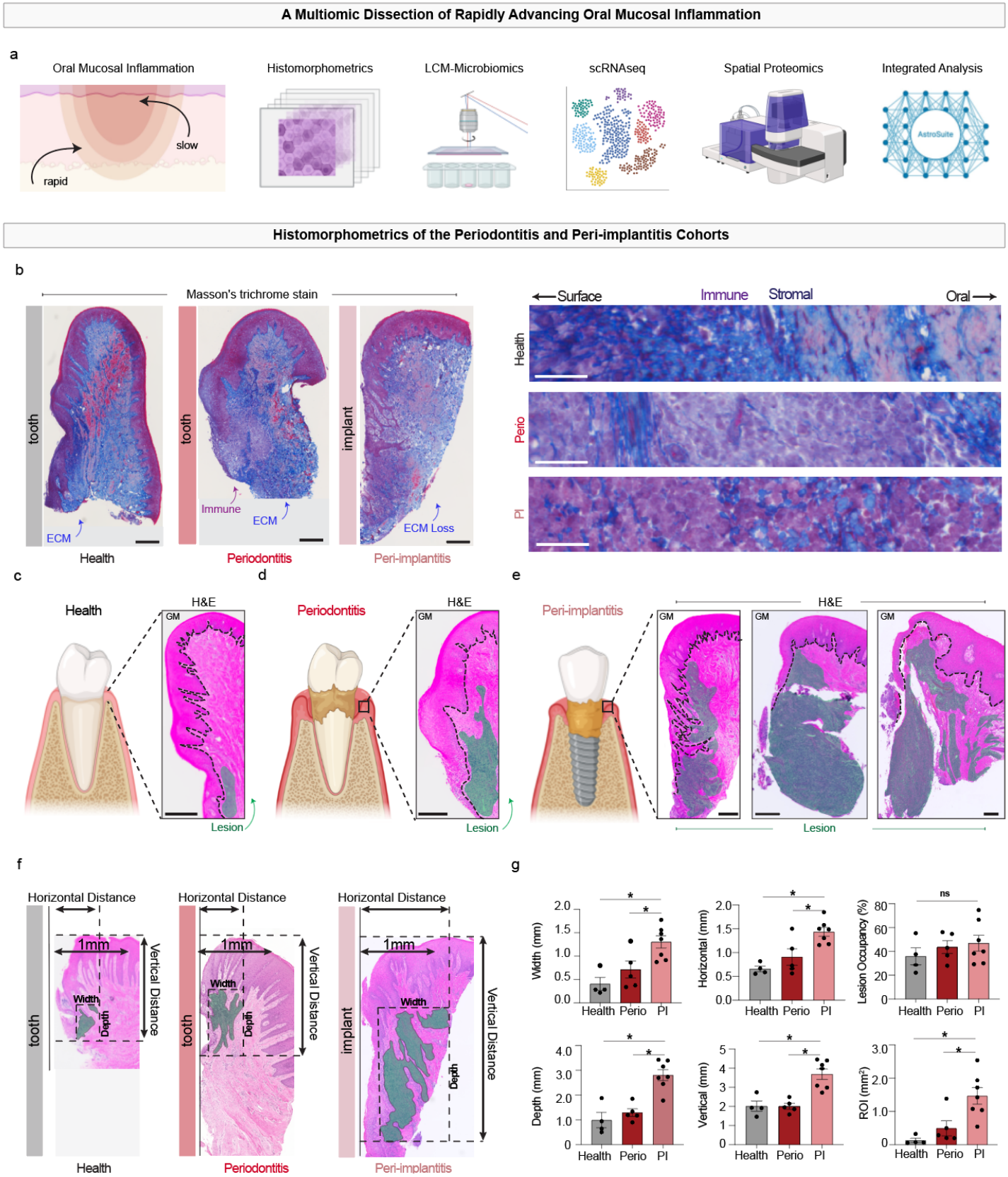
A Multiomic Dissection of Rapidly Advancing Oral Mucosal Inflammation
a
Oral Mucosal Inflammation
slow
rapid
Histomorphometrics
LCM-Microbiomics
scRNAseq
Spatial Proteomics
Integrated Analysis
AstroSuite
Histomorphometrics of the Periodontitis and Peri-implantitis Cohorts
b
Masson's trichrome stain
tooth
ECM
Health
tooth
Immune
ECM
Periodontitis
implant
ECM Loss
Peri-implantitis
Surface
Immune
Stromal
Oral
Health
Perio
PI
c
Health
H&E
GM
Lesion
d
Periodontitis
H&E
GM
Lesion
e
Peri-implantitis
H&E
GM
GM
GM
Lesion
f
Horizontal Distance
1mm
Vertical Distance
Width
Depth
tooth
Health
Horizontal Distance
1mm
Vertical Distance
Width
Depth
tooth
Periodontitis
Horizontal Distance
1mm
Vertical Distance
Width
Depth
implant
Peri-implantitis
g
Width (mm)
Horizontal (mm)
Lesion Occupancy (%)
Depth (mm)
Vertical (mm)
ROI (mm²)
Health
Perio
PI
ns

Figure 1S

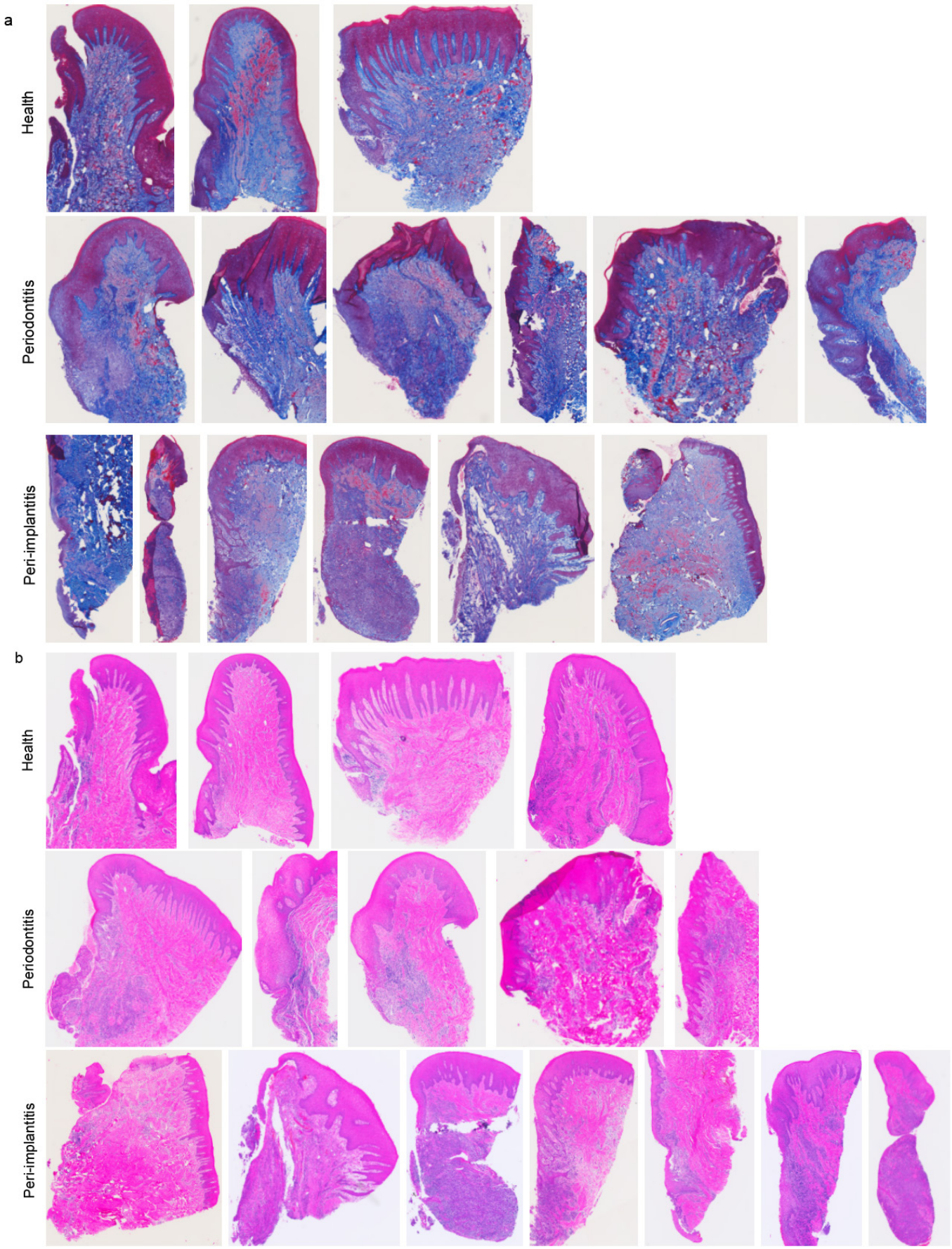
a
Health
Periodontitis
Peri-implantitis
b
Health
Periodontitis
Peri-implantitis

Figure 2

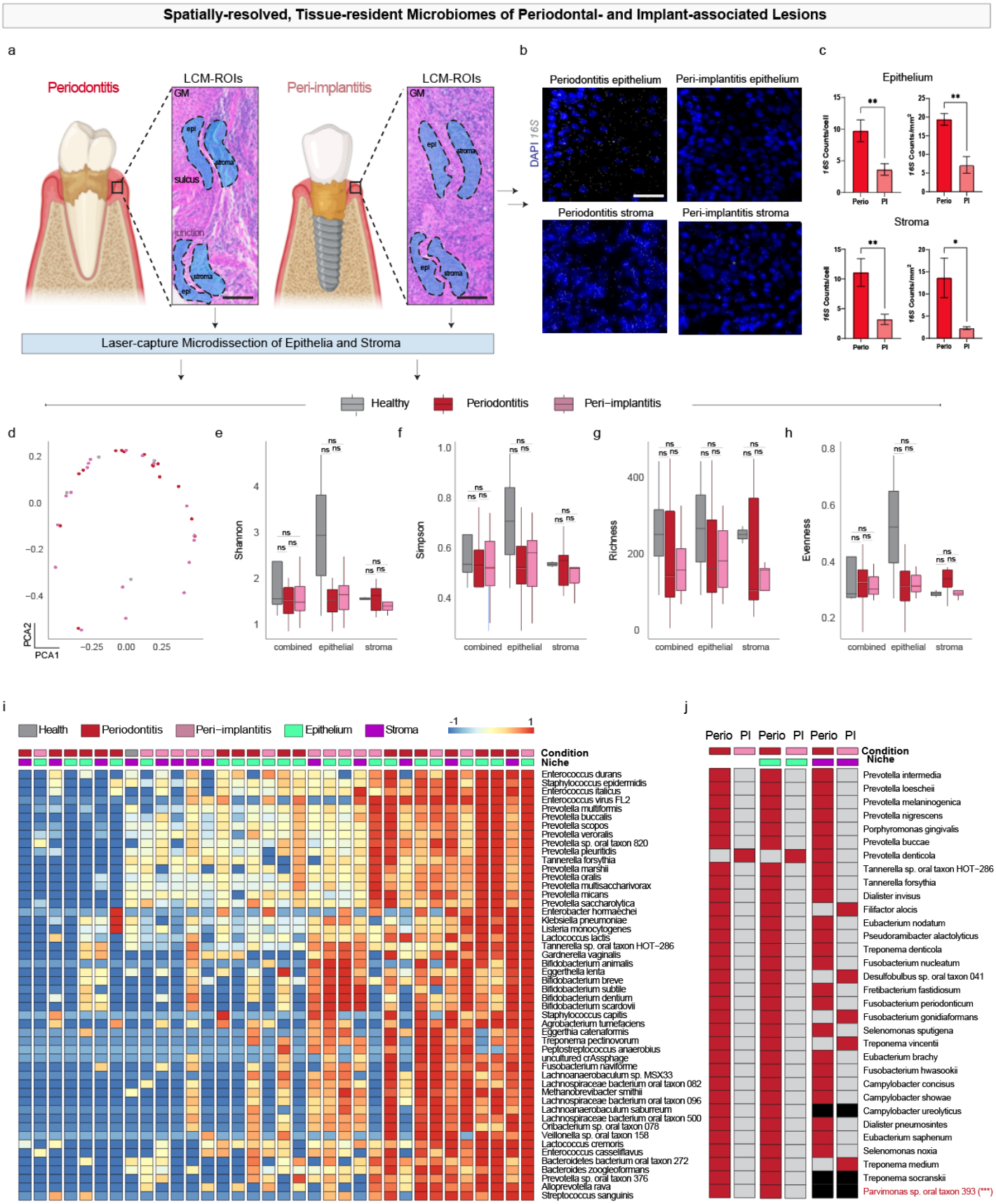
Spatially-resolved, Tissue-resident Microbiomes of Periodontal- and Implant-associated Lesions
a
Periodontitis
LCM-ROIs
Peri-implantitis
LCM-ROIs
GM
epi
stroma
sulcus
junction
Laser-capture Microdissection of Epithelia and Stroma
b
Periodontitis epithelium
Peri-implantitis epithelium
DAPI 16S
Periodontitis stroma
Peri-implantitis stroma
c
Epithelium
Stroma
16S Counts/cell
16S Counts/mm²
Perio
PI
Healthy
Periodontitis
Peri−implantitis
d
PCA2
PCA1
e
Shannon
f
Simpson
g
Richness
h
Evenness
combined
epithelial
stroma
ns
i
Health
Periodontitis
Peri−implantitis
Epithelium
Stroma
Condition
Niche
Enterococcus durans
Staphylococcus epidermidis
Enterococcus italicus
Enterococcus virus FL2
Prevotella multiformis
Prevotella buccalis
Prevotella scopos
Prevotella veroralis
Prevotella sp. oral taxon 820
Prevotella pleuritidis
Tannerella forsythia
Prevotella marshii
Prevotella oralis
Prevotella multisaccharivorax
Prevotella micans
Prevotella saccharolytica
Enterobacter hormaechei
Klebsiella pneumoniae
Listeria monocytogenes
Lactococcus lactis
Tannerella sp. oral taxon HOT−286
Gardnerella vaginalis
Bifidobacterium animalis
Eggerthella lenta
Bifidobacterium breve
Bifidobacterium subtile
Bifidobacterium dentium
Bifidobacterium scardovii
Staphylococcus capitis
Agrobacterium tumefaciens
Eggerthia catenaformis
Treponema pectinovorum
Peptostreptococcus anaerobius
uncultured crAssphage
Fusobacterium naviforme
Lachnoanaerobaculum sp. MSX33
Lachnospiraceae bacterium oral taxon 082
Methanobrevibacter smithii
Lachnospiraceae bacterium oral taxon 096
Lachnoanaerobaculum saburreum
Lachnospiraceae bacterium oral taxon 500
Oribacterium sp. oral taxon 078
Veillonella sp. oral taxon 158
Lactococcus cremoris
Enterococcus casseliflavus
Bacteroidetes bacterium oral taxon 272
Bacteroides zoogleoformans
Prevotella sp. oral taxon 376
Alloprevotella rava
Streptococcus sanguinis
j
Perio
PI
Condition
Niche
Prevotella intermedia
Prevotella loescheii
Prevotella melaninogenica
Prevotella nigrescens
Porphyromonas gingivalis
Prevotella buccae
Prevotella denticola
Tannerella sp. oral taxon HOT−286
Tannerella forsythia
Dialister invisus
Filifactor alocis
Eubacterium nodatum
Pseudoramibacter alactolyticus
Treponema denticola
Fusobacterium nucleatum
Desulfobulbus sp. oral taxon 041
Fretibacterium fastidiosum
Fusobacterium periodonticum
Fusobacterium gonidiaformans
Selenomonas sputigena
Treponema vincentii
Eubacterium brachy
Fusobacterium hwasookii
Campylobacter concisus
Campylobacter showae
Campylobacter ureolyticus
Dialister pneumosintes
Eubacterium saphenum
Selenomonas noxia
Treponema medium
Treponema socranskii
Parvimonas sp. oral taxon 393 (***)

Figure 2S

a

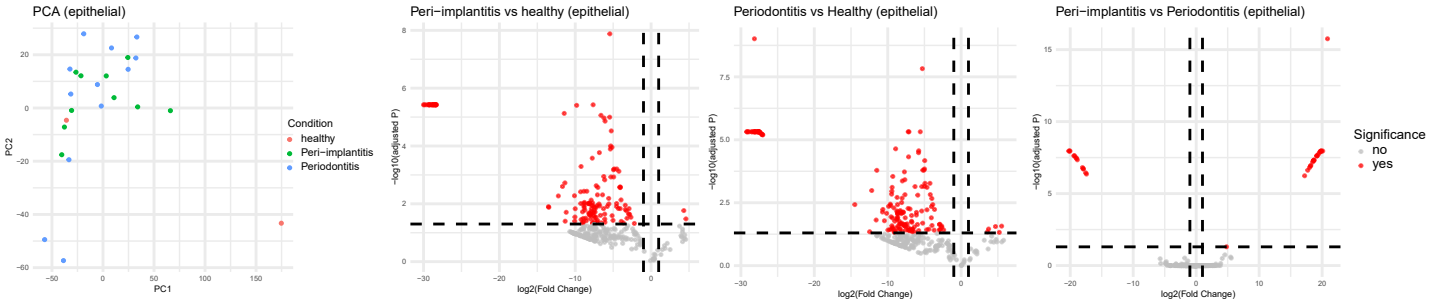
PCA (epithelial)
PC2
PC1
Condition
healthy
Peri−implantitis
Periodontitis
Peri−implantitis vs healthy (epithelial)
−log10(adjusted P)
log2(Fold Change)
Periodontitis vs Healthy (epithelial)
−log10(adjusted P)
log2(Fold Change)
Peri−implantitis vs Periodontitis (epithelial)
−log10(adjusted P)
log2(Fold Change)
Significance
no
yes

b

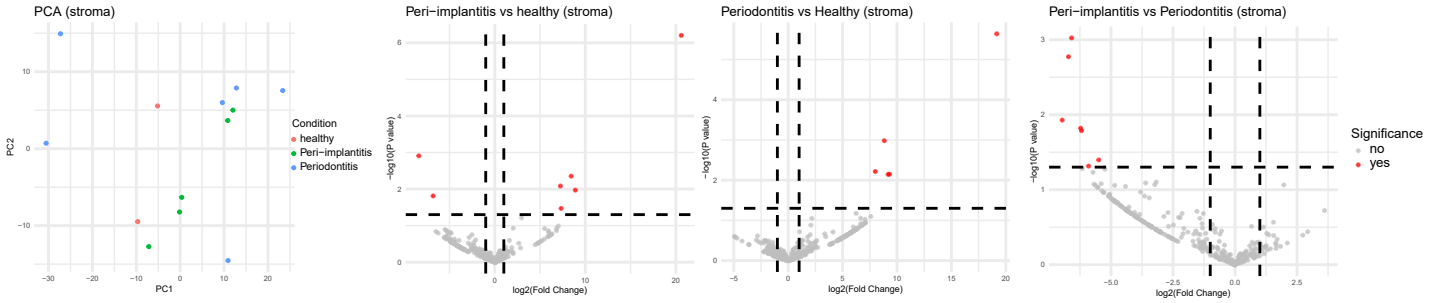
PCA (stroma)
PC2
PC1
Condition
healthy
Peri−implantitis
Periodontitis
Peri−implantitis vs healthy (stroma)
−log10(P value)
log2(Fold Change)
Periodontitis vs Healthy (stroma)
−log10(P value)
log2(Fold Change)
Peri−implantitis vs Periodontitis (stroma)
−log10(P value)
log2(Fold Change)
Significance
no
yes

Figure 3

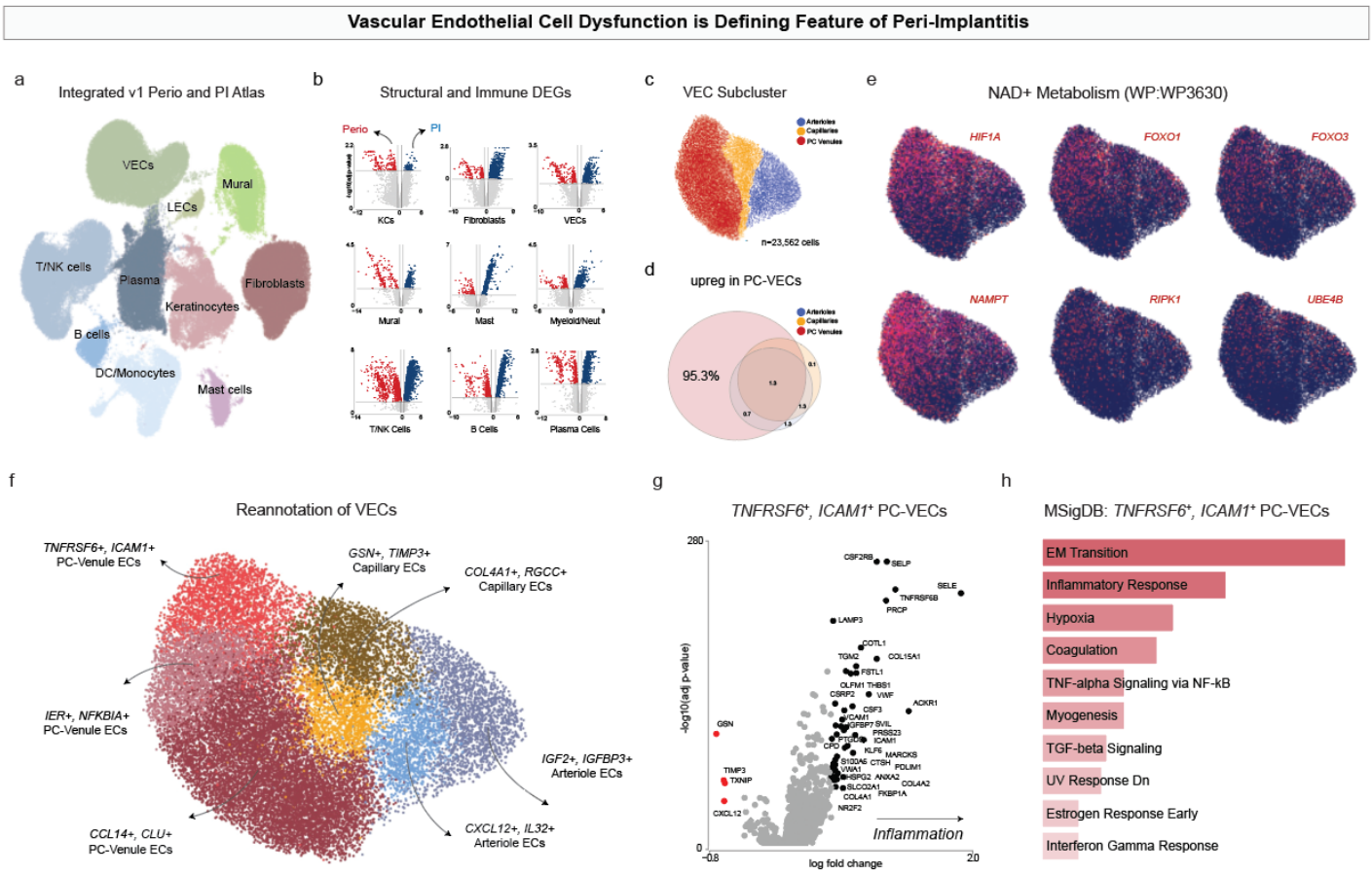
Vascular Endothelial Cell Dysfunction is Defining Feature of Peri-Implantitis
a
Integrated v1 Perio and PI Atlas
VECs
Mural
LECs
T/NK cells
Plasma
Fibroblasts
Keratinocytes
B cells
DC/Monocytes
Mast cells
b
Structural and Immune DEGs
Perio
PI
KCs
Fibroblasts
VECs
Mural
Mast
Myeloid/Neut
T/NK Cells
B Cells
Plasma Cells
c
VEC Subcluster
Arterioles
Capillaries
PC Venules
n=23,562 cells
d
upreg in PC-VECs
95.3%
e
NAD+ Metabolism (WP:WP3630)
HIF1A
FOXO1
FOXO3
NAMPT
RIPK1
UBE4B
f
Reannotation of VECs
TNFRSF6+, ICAM1+
PC-Venule ECs
GSN+, TIMP3+
Capillary ECs
COL4A1+, RGCC+
Capillary ECs
IER+, NFKBIA+
PC-Venule ECs
IGF2+, IGFBP3+
Arteriole ECs
CCL14+, CLU+
PC-Venule ECs
CXCL12+, IL32+
Arteriole ECs
g
TNFRSF6+, ICAM1+ PC-VECs
-log10(adj p-value)
log fold change
Inflammation
GSN
TIMP3
TXNIP
CXCL12
h
MSigDB: TNFRSF6+, ICAM1+ PC-VECs
EM Transition
Inflammatory Response
Hypoxia
Coagulation
TNF-alpha Signaling via NF-kB
Myogenesis
TGF-beta Signaling
UV Response Dn
Estrogen Response Early
Interferon Gamma Response

Figure 3S

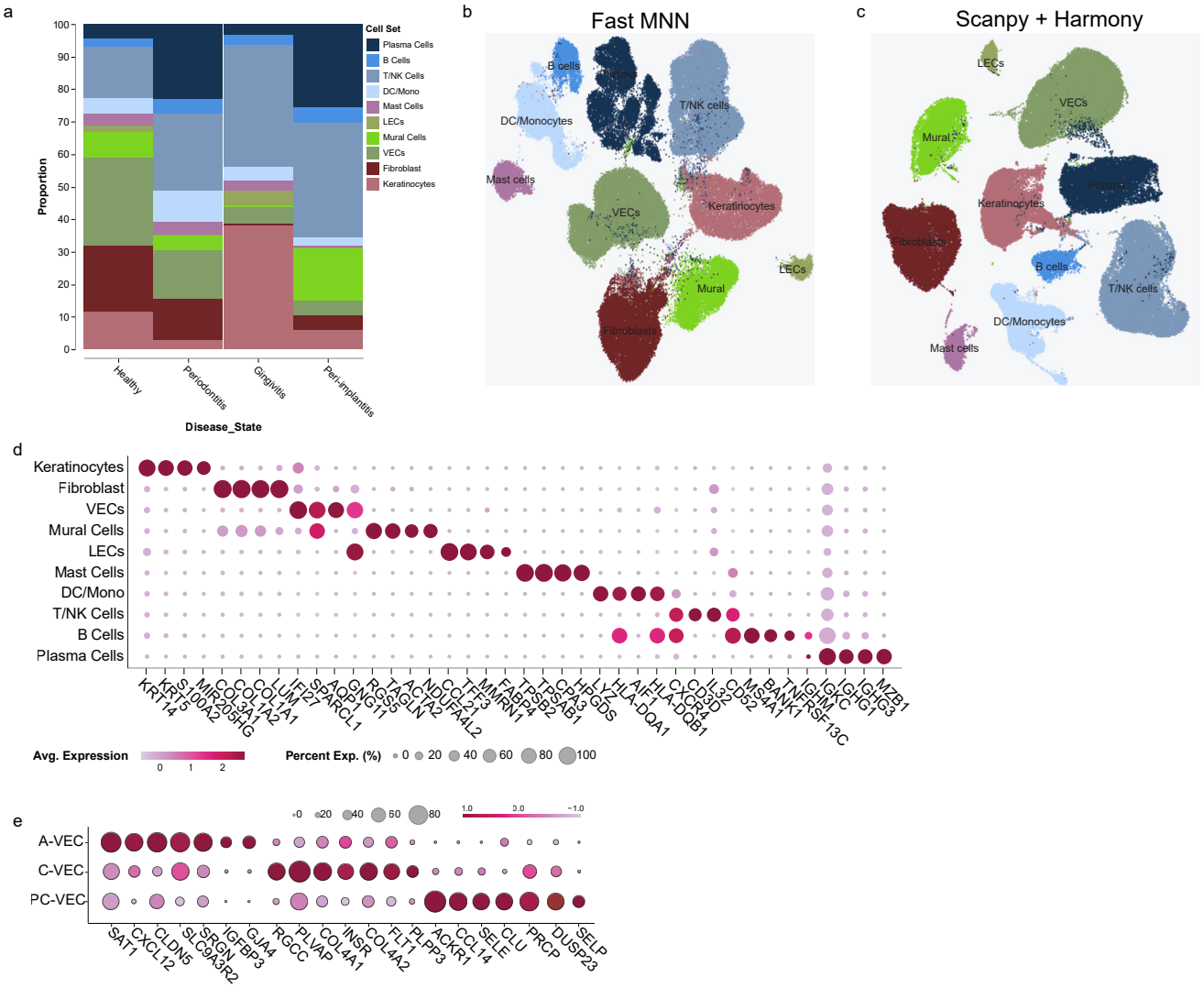
a
Cell Set
Plasma Cells
B Cells
T/NK Cells
DC/Mono
Mast Cells
LECs
Mural Cells
VECs
Fibroblast
Keratinocytes
Proportion
Healthy
Periodontitis
Gingivitis
Peri-implantitis
Disease_State
b
Fast MNN
B cells
T/NK cells
DC/Monocytes
Mast cells
VECs
Keratinocytes
LECs
Mural
Fibroblasts
c
Scanpy + Harmony
LECs
VECs
Mural
Keratinocytes
Fibroblasts
B cells
T/NK cells
DC/Monocytes
Mast cells
d
Keratinocytes
Fibroblast
VECs
Mural Cells
LECs
Mast Cells
DC/Mono
T/NK Cells
B Cells
Plasma Cells
KRT14
KRT5
S100A2
MIR205HG
COL5A1
COL1A2
COL1A1
LUM
IFI27
SPARCL1
AQP1
GNG11
RGS5
TAGLN
ACTA2
NDUFA4L2
CCL21
TFF3
MMRN1
FABP4
TPSB2
TPSAB1
CPA3
HPGDS
LYZ
HLA-DQA1
AIF1
HLA-DQB1
CXCR4
CD3D
IL32
CD52
MS4A1
BANK1
TNFRSF13C
IGHM
IGKC
IGHG1
IGHG3
MZB1
Avg. Expression
0
1
2
Percent Exp. (%)
0
20
40
60
80
100
e
A-VEC
C-VEC
PC-VEC
SAT1
CXCL12
CLDN5
SLC9A3R2
SRGN
IGFBP3
GJA4
RGCC
PLVAP
COL4A1
INSR
COL4A2
FLT1
PLPP3
ACKR1
CCL14
SELE
CLU
PRCP
DUSP23
SELP

Figure 4

Detection of CD38+ Endothelial Remodeling in Peri-implantitis using Spatial Proteomics

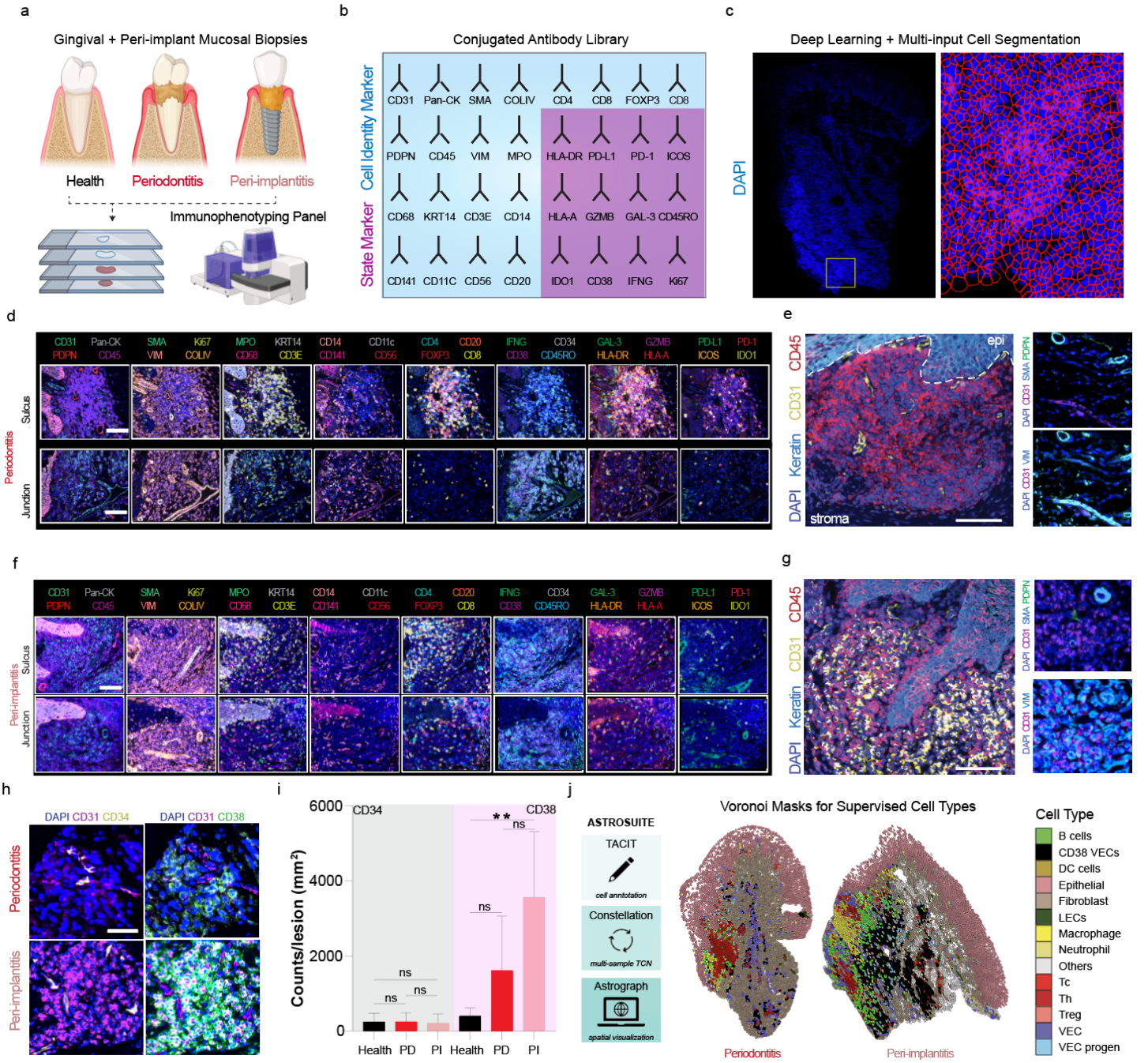

Figure 4S

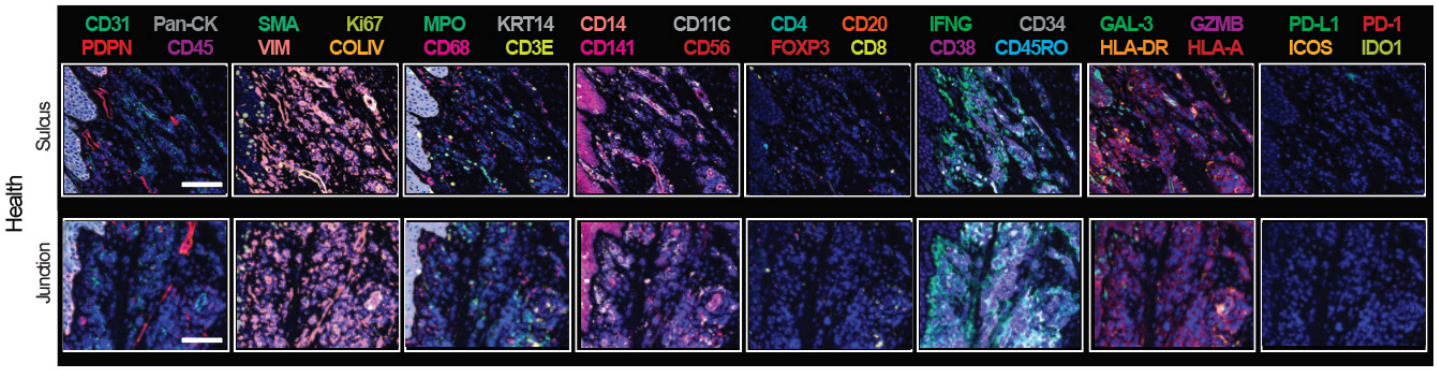
CD31
PDPN
Pan-CK
CD45
SMA
VIM
Ki67
COLIV
MPO
CD68
KRT14
CD3E
CD14
CD141
CD11C
CD56
CD4
FOXP3
CD20
CD8
IFNG
CD38
CD34
CD45RO
GAL-3
HLA-DR
GZMB
HLA-A
PD-L1
ICOS
PD-1
IDO1
Health
Sulcus
Junction

Figure 5

Spatially-distinct CD38+ VEC Neighborhoods Define Peri-implantitis Pathogenesis

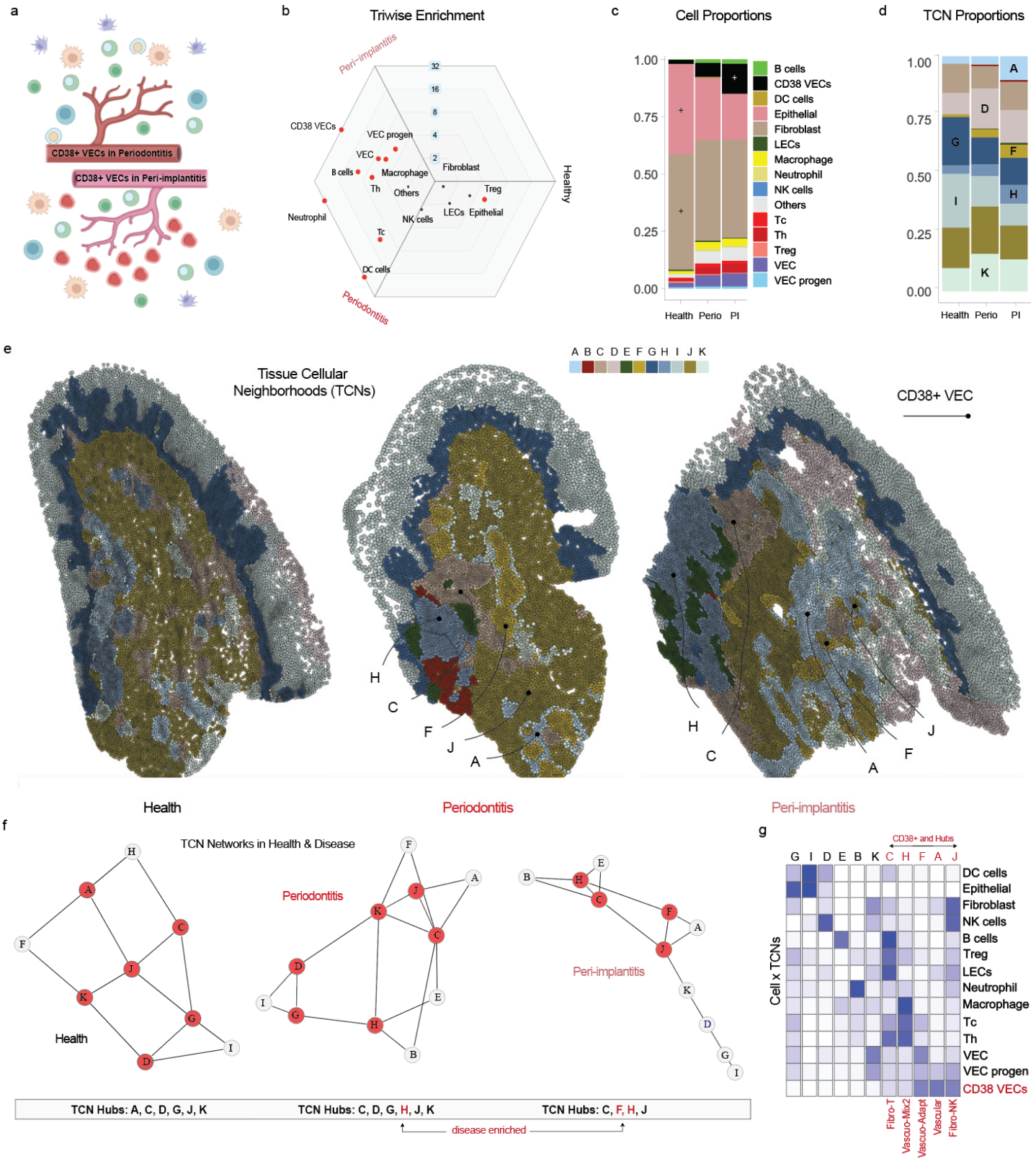

Figure 5S

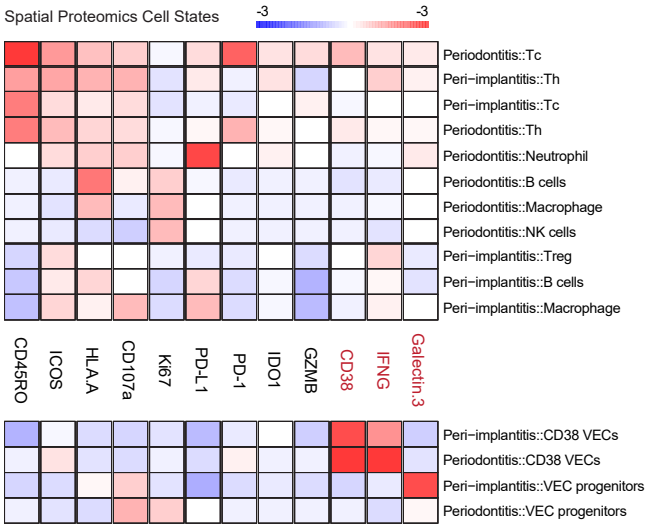
Spatial Proteomics Cell States
-3
-3
Periodontitis::Tc
Peri−implantitis::Th
Peri−implantitis::Tc
Periodontitis::Th
Periodontitis::Neutrophil
Periodontitis::B cells
Periodontitis::Macrophage
Periodontitis::NK cells
Peri−implantitis::Treg
Peri−implantitis::B cells
Peri−implantitis::Macrophage
CD45RO
ICOS
HLA.A
CD107a
Ki67
PD-L1
PD-1
IDO1
GZMB
CD38
IFNG
Galectin.3
Peri−implantitis::CD38 VECs
Periodontitis::CD38 VECs
Peri−implantitis::VEC progenitors
Periodontitis::VEC progenitors

Figure 6
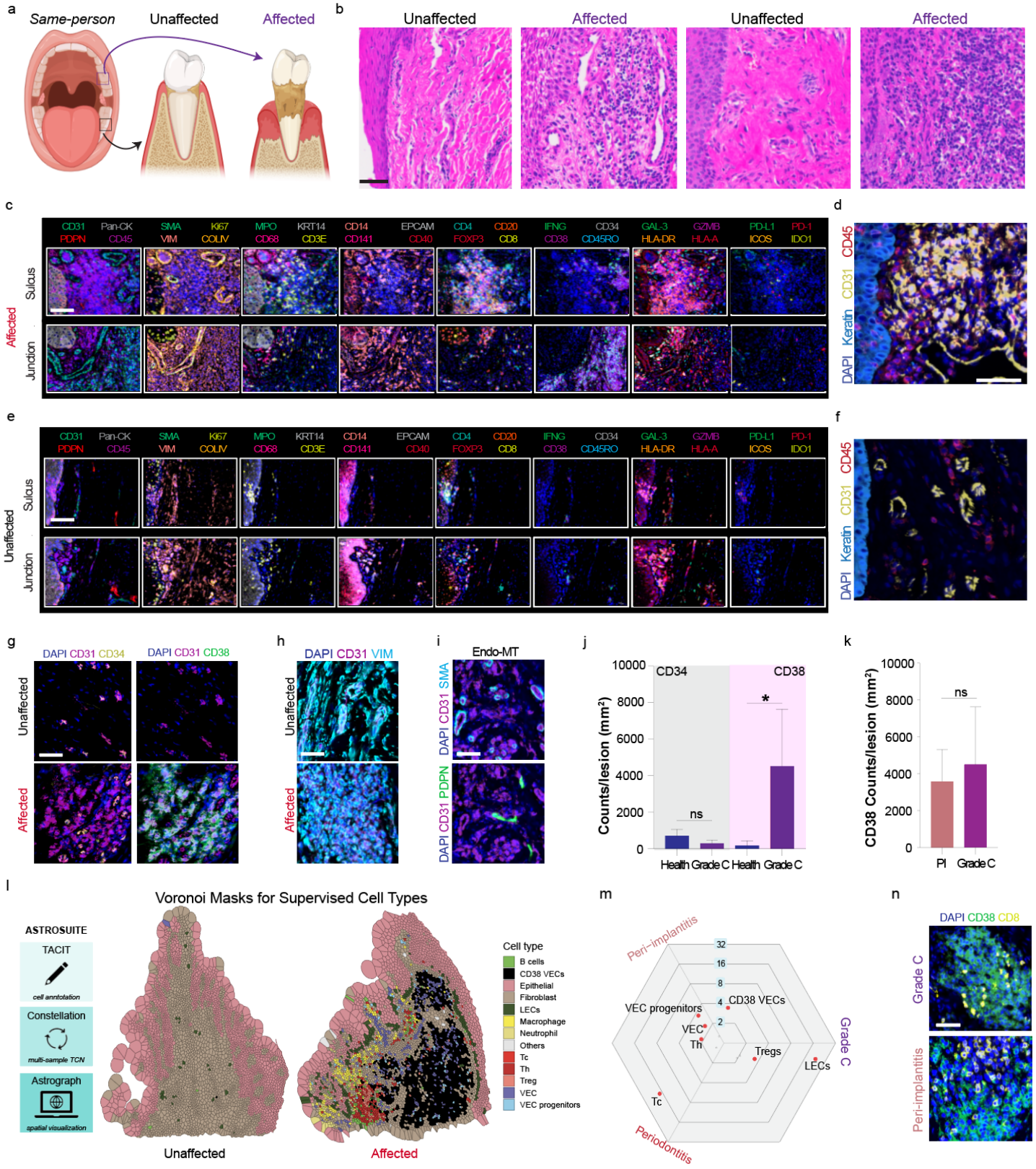
Dectection of CD38+ Vasculopathy in Stage III/Grade C Periodontitis using Spatial Proteomics